2018

U-Pb and Hf Isotopic Evidence for an Arctic Origin of Terranes in Northwestern Washington

Elizabeth R. Schermer
Western Washington University, liz.schermer@wwu.edu

Eric A. Hoffnagle
Western Washington University

Edwin H. Brown
Western Washington University, ned.brown@wwu.edu

George E. Gehrels

William C. McClelland

Recommended Citation

Schermer, E.R., Hoffnagle, E.A., Brown, E.H., Gehrels, G.E., and McClelland, W.C., 2018, U-Pb and Hf isotopic evidence for an Arctic origin of terranes in northwestern Washington: Geosphere, v. 14, no. 2, p. 1–26, doi:10.1130/GES01557.1.

Research Paper

GEOSPHERE

GEOSPHERE; v. 14, no. 2

doi:10.1130/GES01557.1

15 figures; 1 supplemental file

CORRESPONDENCE: liz.schermer@wwu.edu

CITATION: Schermer, E.R., Hoffnagle, E.A., Brown, E.H., Gehrels, G.E., and McClelland, W.C., 2018, U-Pb and Hf isotopic evidence for an Arctic origin of terranes in northwestern Washington: Geosphere, v. 14, no. 2, doi:10.1130/GES01557.1.

Science Editor: Raymond M. Russo
Associate Editor: G. Lang Farmer

Received 15 May 2017
Revision received 16 October 2017
Accepted 4 January 2018

U-Pb and Hf isotopic evidence for an Arctic origin of terranes in northwestern Washington

Elizabeth R. Schermer[1], Eric A. Hoffnagle[1,*], Edwin H. Brown[1], George E. Gehrels[2], and William C. McClelland[3]

[1]Geology Department, Western Washington University, MS9080, 516 High Street, Bellingham, Washington 98225, USA
[2]Department of Geosciences, University of Arizona, 1040 4th Street, Tucson, Arizona 85721, USA
[3]Department of Earth and Environmental Sciences, University of Iowa, 115 Trowbridge Hall, Iowa City, Iowa 52242, USA

ABSTRACT

New field, U-Pb, and Lu-Hf zircon data constrain the geologic history, age, and origin of the Yellow Aster Complex (YAC) in northwestern Washington, providing insight into the tectonic history of this and related Paleozoic arc terranes of the western North American Cordillera. Mapping shows that the oldest YAC rocks consist of quartzofeldspathic paragneiss (meta-arkose) and quartzose calc-silicate paragneiss (metacalcareous siltstone) in gradational contact. Paragneisses are cut by syn-tectonic and post-tectonic intrusions and faulted against granitic orthogneiss. U-Pb zircon results show that (1) maximum depositional ages of paragneisses are Silurian to Early Devonian (432–390 Ma); (2) detrital zircons from quartzose calc-silicate paragneisses show a broad age peak from 1900 to 1000 Ma, while quartzofeldspathic paragneisses contain several distinct Precambrian age peaks, including at 2.0–1.8 Ga and 2.5–2.4 Ga; (3) paragneisses contain early Paleozoic grains with peaks ca. 420–400 and ca. 460–440 Ma; (4) pre-tectonic orthogneiss and syn-tectonic and post-tectonic dikes range from ca. 410–406 Ma; and (5) intrusive rocks contain apparently xenocrystic ca. 480–440 Ma grains. Lu-Hf isotope data show that nearly all Paleozoic zircons have negative $\varepsilon Hf_{(t)}$ values, and zircons in the meta-arkose samples are more negative than those in the calc-silicate. Zircons in several meta-arkose samples yield $\varepsilon Hf_{(t)}$ values of –40 to –57, rare in the North American Cordillera, and requires the involvement of Mesoarchean to Eoarchean crustal components. The most likely source region with crust as old as Eoarchean and early Paleozoic magmatism is the Greenland Caledonides, which implies derivation from the Arctic margin of northeastern Laurentia or Baltica. The chemistry and petrology of the igneous rocks suggest that the terrane was in a continental arc setting before, during, and after deposition of the sedimentary rocks. The data constrain deformation, metamorphism, and magmatism in the YAC to a brief period in the Early Devonian, from ca. 410 to 400 Ma. Age and Hf patterns of the YAC are similar to elements of the Yukon-Tanana and Alexander terranes. Our study shows that the complex history of metamorphosed terranes requires analysis of multiple isotopic and petrologic proxies, and U-Pb analysis of both igneous (n = 50) and detrital (n = 400) zircons to confirm or refute terrane and provenance correlations.

*Current address: Reservoir Group, 510 Guhn Road, Houston, Texas 77040, USA

INTRODUCTION

A growing body of evidence suggests that early Paleozoic arc terranes currently in the North American Cordillera in the Klamath Mountains (California), Cascades Mountains (Washington), and Coast Mountains of Alaska and British Columbia originated in the Arctic region of Laurentia, Baltica, or the Caledonides (e.g., Gehrels et al., 1996; Wright and Wyld, 2006; Colpron and Nelson, 2009, 2011; Miller et al., 2011; Beranek et al., 2013a, 2013b; White et al., 2016). Understanding the origin of these terranes bears on our understanding of the timing and nature of the transition of the western Laurentian margin from a passive to active margin. Migration of terranes to their present sites and final emplacement on the margin during the Mesozoic remain poorly understood processes. Colpron and Nelson (2009) and Wright and Wyld (2006) proposed two different models for the origin of the Paleozoic rocks now part of various terranes. The Northwest Passage model (Colpron and Nelson, 2009, 2011) describes evidence for the Baltican and Siberian origins of several terranes in western North America (e.g., Yreka, Northern Sierra, Alexander) (Fig. 1), wherein terranes originating in the northern Scandinavian Caledonides in pre-Devonian time traveled westward through a northwest passage between the Arctic margins of Laurentia and Siberia to the western margin of Laurentia. Terranes moved westward along a Scotia-style arc and transform system to the eastern margin of the Panthalassa Ocean, where they subsequently evolved in a fringing-arc setting during Devonian time (Colpron and Nelson, 2009). Late Paleozoic and Mesozoic events moved the terranes south, and eventually emplaced them against western North America. An alternative model (Wright and Wyld, 2006) also recognizes the Caledonian affinity of some of these same terranes, but argues that they originated on the Gondwana margin and migrated southward and westward along eastern Laurentia and then northward along western Laurentia. A possibility that the terranes migrated across the Panthalassa Ocean from Asian or Australian homelands has been considered by some, but is not favored based on paleomagnetic data and faunal provenance (Gehrels et al., 1996; Soja, 2008).

A key to understanding the evolution of the Cordilleran margin is in recent work suggesting that several of the pericratonic terranes (or parts of them) have connections to both western Laurentia and western Baltica or eastern Laurentia at the same time, based on their detrital zircon signatures and geo-

Figure 1. Terrane map of the northern Cordillera (after Colpron and Nelson, 2009; Brown et al., 2010). Colors indicate parautochthon, western Laurentian affinity, and Baltic-Caledonian affinity terranes. Ocean-floor rocks, accretionary wedge, and arc terranes derived from Panthalassa are shown. Abbreviations of units mentioned in text: AX—Alexander; B—Belt; CC—Cache Creek; CPC—Coast Plutonic Complex; Cz—Cenozoic cover; EK—Eastern Klamath; GC—Golconda; NA—North America; NS—Northern Sierra; OK—Okanagan; QN—Quesnellia; RM—Roberts Mountains; SM—Slide Mountain; SN—Sierra Nevada batholith; ST—Stikine; WR—Wrangellia; YK—Yreka; YT—Yukon Tanana. AK—Alaska; B.C.—British Columbia.

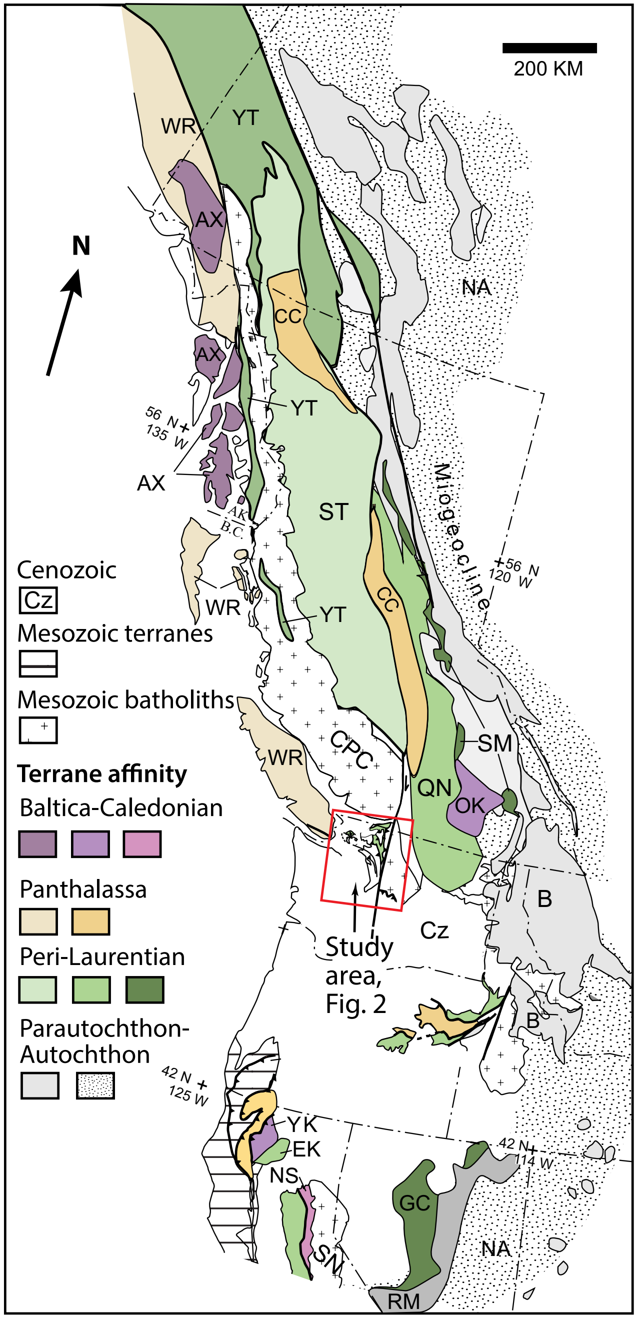

logic history (Wright and Wyld, 2006; Wright and Grove, 2009; Brown et al., 2010; Tochilin et al., 2014; Pecha et al., 2016). In addition, upper Devonian rocks of the Cordilleran passive margin and Antler foredeep contain west-derived non-Laurentian debris (e.g., Stevenson et al., 2000; Wright and Grove, 2009; Brown et al., 2010; Beranek et al., 2016), suggesting arrival of terranes off western Laurentia by that time. Distinguishing what is truly an exotic terrane from a pericratonic basinal deposit that received debris from an approaching or accreting terrane is necessary to understand the timing of terrane accretion. Some of the pericratonic terranes, including the Chilliwack composite terrane (Figs. 1 and 2), the focus of this study, contain evidence for pre-Devonian deformation, metamorphism, and magmatism (unknown in western Laurentia), together with Early Devonian and older detritus from western Laurentia (Brown et al., 2010). An Early Devonian link between Baltican terranes and western North America would place severe constraints on models that propose a Late Devonian arrival of exotic terranes (Wright and Wyld, 2006; Colpron and Nelson, 2009). This apparently contradictory evidence is a problem addressed in our study. We also consider broader tectonic models to explain deformation within terranes and the timing and tectonic setting of magmatism.

We use field mapping of the Yellow Aster Complex (YAC; YA in Fig. 2), the basement of the Chilliwack terrane, together with combined U-Pb and Lu/Hf analysis on zircons, to interpret age, provenance, and geologic history to address the following questions.

1. Is the pericratonic signature in the Chilliwack terrane definitively western Laurentian (i.e., is it related to Yukon-Tanana, as proposed by Brown et al., 2010)?

2. Is the Alexander terrane present in western Washington as part of the Chilliwack composite terrane, or does the Chilliwack terrane contain debris shed from the Alexander terrane into a basin off the coast of western or Arctic Laurentia (e.g., Hoffnagle, 2014; Hoffnagle et al., 2014)? In addition to defining an important element of the Paleozoic tectonic evolution, this question has implications for Mesozoic reconstruction of the Cordillera, because the Chilliwack terrane had a Mesozoic history very different from that of the Yukon-Tanana and Alexander terranes.

3. What is the timing and significance of Paleozoic magmatism, deformation, and metamorphism in the YAC? Are these events that occurred in a Caledonian setting, later transported to western Laurentia, something that occurred during transit, or is this a previously unrecognized, perhaps local, event that occurred while the terrane was adjacent to western Laurentia?

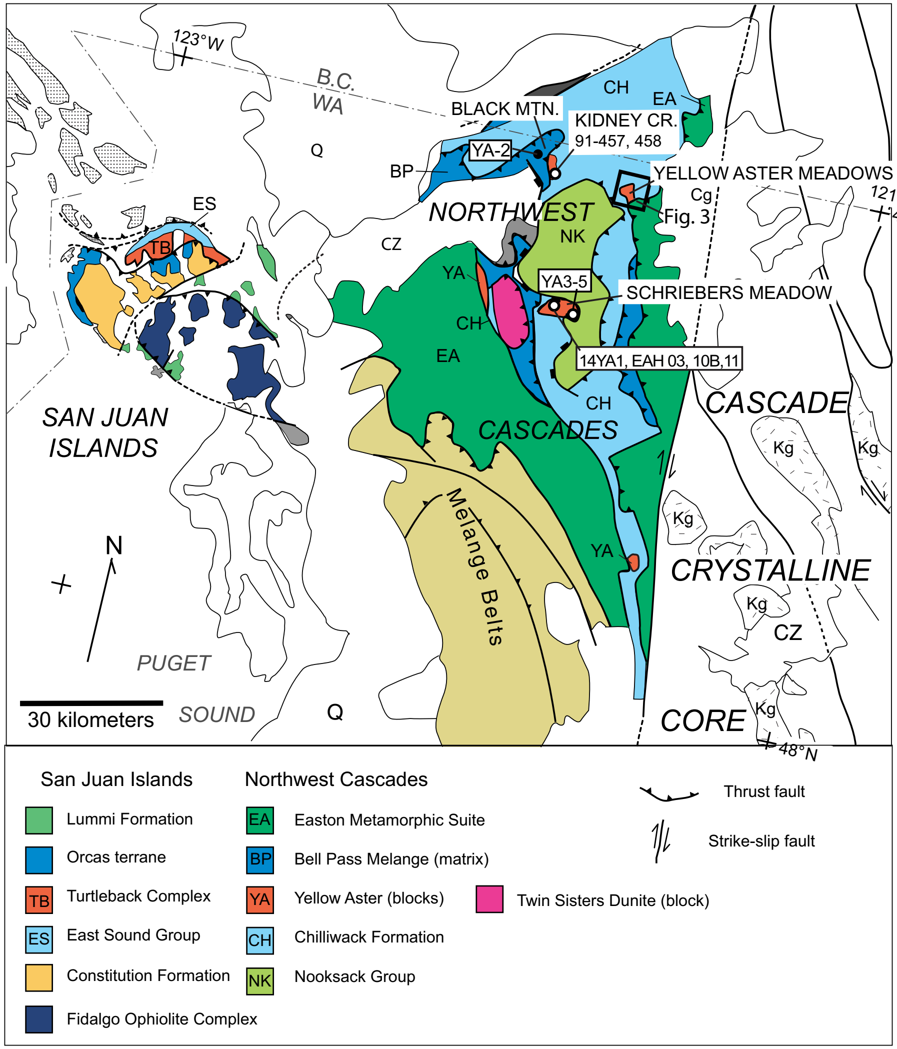

Figure 2. Geologic setting of Chilliwack composite terrane showing Northwest Cascades thrust system and correlative San Juan Islands thrust system. Uncolored areas are unrelated and/or younger units. Abbreviations not indicated in legend: B.C.—British Columbia, CZ—Cenozoic cover, Q—Quaternary units, Cg—Cenozoic granitic rocks, Kg—Cretaceous granitic rocks. WA—Washington; MTN.—mountain; CR.—Creek. Chilliwack composite terrane includes CH, ES, TB, and YA. Box shows location of map in Figure 3. Samples not shown in Figure 3 are labeled here; open circles are from this study, closed circle is from Brown and Gehrels (2007). Map is modified from Brown et al. (2010).

GEOLOGIC AND TECTONIC SETTING OF THE YAC

Breakup of Rodinia in Neoproterozoic time led to development of the Cordilleran passive margin along the western edge of Laurentia (Fig. 1). Late Proterozoic to Paleozoic passive margin strata have been extensively studied, and their detrital zircons record erosion of the western Laurentian craton, with a characteristic pattern of Precambrian zircon ages that varies somewhat from north to south (Gehrels et al., 1995, 2000; Gehrels and Ross, 1998; Gehrels and Pecha, 2014). Paleozoic through Cenozoic orogenic events have displaced the passive margin rocks, but their parautochthonous heritage is recorded in stratigraphic, faunal, and detrital zircon characteristics. Terranes outboard of the parautochthonous rocks contain some ties to western North America, but their Paleozoic and Mesozoic geological histories record separation from the continent by oceanic basins of variable, but possibly large, extent. These peri-Laurentian or pericratonic terranes are thought to have formed as the continental margin was rifted during Devonian time to form the Slide Mountain ocean, with a subduction zone and island arc at its outer edge (Rubin et al., 1990a; Gehrels et al., 1991; Colpron and Nelson, 2009). The peri-Laurentian fringing arc terranes include the Yukon-Tanana, Stikinia, and Quesnellia (Fig. 1). The Chilliwack composite terrane of Washington and southern British Columbia (as defined in Brown et al., 2010) has long been thought to be broadly correlative with these Paleozoic arc terranes (Brown and Vance, 1987; Brandon et al., 1988).

A belt of terranes that have few ties to western North America until late Mesozoic time lies outboard of the pericratonic terranes. The origin and displacement history of these more exotic terranes are controversial. One of the largest, the Alexander terrane (Fig. 1), has been interpreted to have its origins in western Baltica, based on the timing of orogenic events, detrital zircon signature, paleomagnetism, and paleontology (Bazard et al., 1995; Butler et al., 1997; Gehrels et al., 1996; Soja and Antoshkina, 1997; Grove et al., 2008; Beranek et al., 2012, 2013a, 2013b; Tochilin et al., 2014; White et al., 2016). The Alexander terrane is thought to have been accreted to the western Yukon-Tanana terrane prior to Middle Jurassic time (van der Heyden, 1992; McClelland et al., 1992); however, final attachment to western North America may not have occurred until Cretaceous time (Crawford et al., 1987; Rubin et al., 1990b; Rubin and Saleeby, 1992).

The Chilliwack composite terrane (Fig. 2) consists of three elements: (1) metamorphic basement in the North Cascades (the YAC), consisting of metamorphosed quartzose and carbonate sediments intruded by Silurian to Devonian mafic to felsic plutonic rocks (YA in Fig. 2), (2) plutonic basement in the San Juan Islands, consisting of Ordovician(?)–Devonian gabbroic and tonalitic plutonic basement (Turtleback Complex; TB, Fig. 2) of possible arc affinity, and (3) Early Devonian and younger volcanic and volcaniclastic sedimentary rocks (Chilliwack and East Sound Groups, CH and ES, respectively) (Figs. 2 and 3; Brown et al., 2010). Work by Brown et al. (2010) and Hoffnagle et al. (2014) suggests lithologic and age similarities to both Baltican and Laurentian terranes, and possible mixing of sediment derived from both sources. In this study we focus on the YAC to evaluate the geologic and tectonic history and origin of the basement of the Chilliwack composite terrane.

GEOLOGY OF THE YAC

Previous Work

The YAC consists of kilometer-scale fault-bound tectonic blocks that crop out within the North Cascades thrust system (Fig. 2). Early workers defined the YAC as an orthogneiss (Misch, 1966; Mattinson, 1972) while later work recognized pyroxene, quartzose, and calc-silicate paragneisses in addition to orthogneiss and unfoliated intrusives (Blackwell, 1983; Brown, 1987; Rasbury

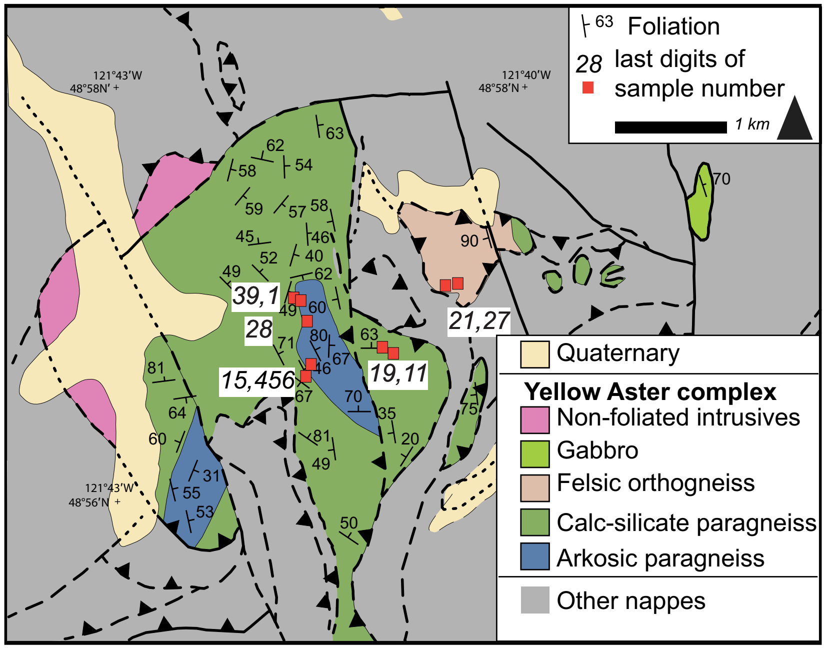

Figure 3. Geologic map of Yellow Aster Meadows area, from this study and modified from Sevigny (1983) and Tabor et al. (2003). Geochronology samples are shown in red boxes.

and Walker, 1992; Tabor et al., 2003). Although most paragneisses are nearly completely recrystallized, detrital textures are preserved locally. The protoliths have been interpreted as quartzose-arkosic sands and carbonates that were deposited on a passive margin (Brown and Dragovich, 2003; Brown et al., 2010). Intrusive rocks crosscut the paragneisses. Although orthogneiss is present, undeformed intrusions predominate (e.g., Blackwell, 1983; Sevigny, 1983; Brown et al., 2010). The undeformed intrusions comprise a wide range of grain sizes and compositions, from granite and rhyolite to gabbro and basalt. The paragneissic rocks of the YAC were metamorphosed to amphibolite facies with a later greenschist facies overprint (Misch, 1966; Mattinson, 1972; Brown et al., 1981; Sevigny, 1983). High-grade metamorphism ca. 415 Ma was inferred from a concordant U-Pb date on sphene (Mattinson, 1972).

Determining the age of the YAC has been problematic. The earliest radiometric dates suggested a possible Precambrian age for the paragneisses, together with Paleozoic arc magmatism based on discordant ages on paragneissic rocks and sparse ages on felsic intrusions (Mattinson, 1972; Rasbury and Walker, 1992). Detrital zircon dating of one quartzose paragneiss sample (YA2, Fig. 2) yielded predominantly Proterozoic ages, with the two youngest zircons ca. 1000 Ma (Brown and Gehrels, 2007). Two post-tectonic intrusions (YA3, YA4, Fig. 2) were dated as 418 and 410 Ma (Brown et al., 2010). The U-Pb and lithologic data led to the suggestion (Brown and Gehrels, 2007; Brown et al., 2010) that the paragneiss was derived from Ordovician passive margin strata deposited along western Laurentia. Intrusions of similar age (418–375 Ma) (Mattinson, 1972; Whetten et al., 1978; Brown et al., 2010) and composition in the Turtleback Complex in the San Juan Islands led workers to correlate the two terranes as part of an early Paleozoic arc complex (Brown and Vance, 1987; Brandon et al., 1988; Brown et al., 2010). The YAC and Turtleback complex are interpreted as the basement to a cover of correlated Devonian to Permian volcanic and sedimentary units (Chilliwack and East Sound Groups; Fig. 2) in the Chilliwack composite terrane (Brown et al., 2010).

The YAC occurs as kilometer-scale tectonic blocks within the Bell Pass mélange, a very low grade tectonic assemblage that also includes blocks of metamorphosed chert, phyllite, metavolcanic rock, metagraywacke, and ultramafic rock (Fig. 2). The youngest components of the mélange (late Early Cretaceous sandstone) and age constraints on faulting (ca. 90 Ma) (Brown and Gehrels, 2007; Brown, 1987) indicate a Late Cretaceous thrust setting. Although controversy exists around the kinematics of thrusting (e.g., Brown, 1987; McGroder, 1991; Cowan and Brandon, 1994; Brown, 2012), the brittle character and very low grade of metamorphism do not affect consideration of the provenance and internal crosscutting relationships of rocks within the YAC. We are, however, unable to use kinematic data from the metamorphic tectonites of the YAC to interpret the deformational history because blocks have likely been reoriented during Cretaceous thrusting. The presence of the YAC in the low-grade mélange is, however, fortunate for our understanding of Paleozoic events, as similar terranes to the north and south have been intruded by Jurassic–Cretaceous plutons of the Coast Plutonic Complex and Sierra Nevada batholiths (Fig. 1), obscuring their older history.

New Mapping

In this study we focused our mapping and sampling on the largest exposures of the YAC in the vicinity of Yellow Aster Meadows and Schreiber's Meadow (Figs. 2 and 3). Additional sampling was conducted at road cuts near Kidney Creek and Schreiber's Meadow (Fig. 2). Paragneiss is cut by a wide array of small, unfoliated dikes, sills, and irregularly shaped intrusive bodies that are not dated and are not shown in Figure 3. In our detailed map area, orthogneiss occurs in a tectonic block separate from the majority of the paragneiss (Fig. 3).

The paragneiss unit consists of intercalated quartzose calc-silicate paragneiss, quartzofeldspathic paragneiss, and local marble and quartzite. Local exposures of an augen gneiss with a possible volcanic protolith were also observed, consistent with earlier observations of Brown et al. (2010). We discovered low-strain rocks that add significant constraints on the metasedimentary sequence, especially with regard to the two most abundant rock types, the quartzose calc-silicate paragneiss and quartzofeldspathic paragneiss.

Quartzose Calc-Silicate Paragneiss

Fine-grained quartzose calc-silicate paragneiss contains continuous quartz- and plagioclase-rich layers alternating with diopside-rich layers. These layers define millimeter-scale mylonitic to gneissic foliation (Fig. 4A). Typically, the calc-silicate contains at least 25% quartz (commonly >50%) with variable amounts of plagioclase (15%–25%), diopside (10%–25%), and epidote (10%–15%). Less abundant minerals include tremolite-actinolite, calcite, and titanite. Calc-silicate paragneiss is interbedded with quartzite and marble (Fig. 4B). Contacts between these lithologies are typically sharp. Evidence of varying strain intensity in quartz-rich layers includes recrystallized quartz, subgrains, and quartz ribbons with undulose extinction. Unstrained quartz grains are rare, but weakly strained unrecrystallized grains are locally abundant. Diopside is locally strained and partially reacted to epidote and actinolite. Detrital textures are locally preserved, including rounded monocrystalline quartz grains and polycrystalline grains interpreted as felsic plutonic clasts (Fig. 4C).

Quartzofeldspathic Paragneiss (Arkosic Paragneiss)

Quartzofeldspathic paragneiss is characterized by a high percentage of quartz (>60%), locally abundant coarse feldspar, and a general lack of clinopyroxene. Other minerals in this lithology include variable amounts of plagioclase (10%–25%), K-feldspar (5%–10%), muscovite (5%–15%), and chlorite (5%–15%). Trace amounts of metamorphic garnet, typically fractured and partially replaced by chlorite, are also present. Quartzofeldspathic paragneiss typically has ~5-mm-thick layering and is medium to coarse grained. Some outcrops consist of centimeter-scale alternating bands of feldspar- and quartz-rich layers that appear to preserve detrital textures (Fig. 4D).

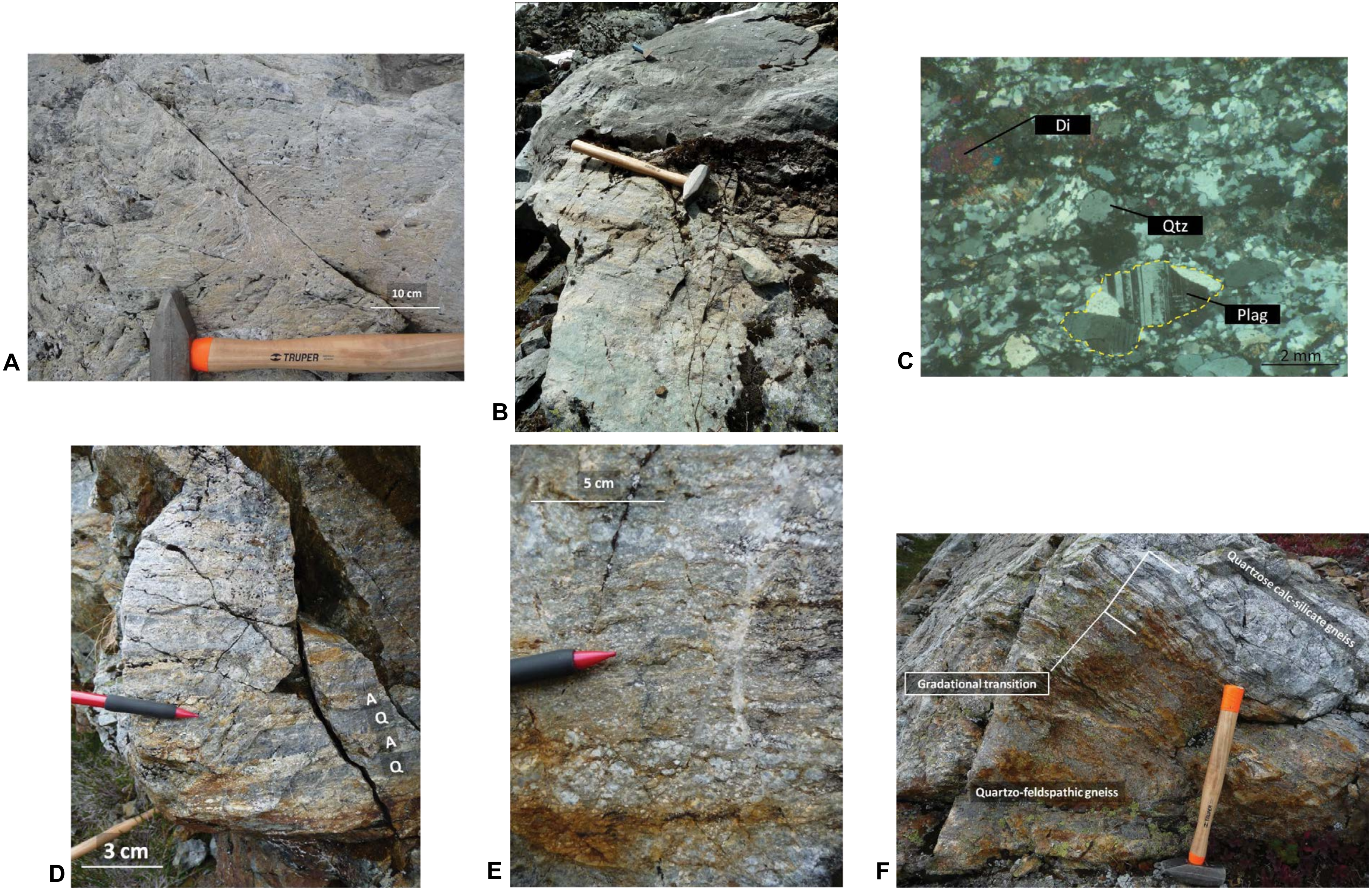

Figure 4. Photographs of representative Yellow Aster Complex (YAC) paragneiss samples. (A) Outcrop photograph of folded calc-silicate paragneiss. Gneissic layers are ~1–2 mm thick. Photograph is from the Yellow Aster Butte study area near sample 14YA19. (B) Block of calc-silicate paragneiss with marble contact. Marble is above the hammer. Hammer is 38 cm long. Photo from the Schriebers Meadow field area. Sample EAH11. (C) Sample EAH39, cross-polarized light photomicrograph of calc-silicate paragneiss. Foliated texture contains fine-grained recrystallized quartz, coarse-grained rounded quartz (Qtz), and subangular plagioclase (Plag) grains. A polycrystalline grain is outlined. Coarse rounded grains are interpreted as relict detrital grains. Di—Diopside. (D) Arkosic paragneiss (14YA28) with alternating feldspar-rich (A) and quartz-rich (Q) layers, Yellow Aster Meadows. (E) Arkosic paragneiss showing compositional layering and a variety of grain sizes. White and coarse grains are plagioclase. (F) A gradational contact between quartzofeldspathic and quartzose calc-silicate paragneisses, interpreted as premetamorphic. Hammer is 38 cm long.

Owing to the abundance of feldspar (Fig. 4E) and the common presence of grain size and compositional layering, we call this unit arkosic paragneiss. Quartz is mostly fine to medium grained and recrystallized. Larger quartz ribbons are also present, and nearly all coarse-grained quartz is strained, showing signs of undulatory extinction and subgrains.

At Yellow Aster Meadows the contact between the two types of paragneiss is exposed as a foliation-parallel interlayering (Figs. 4F and 5). Contacts between the different paragneisses are both abrupt and gradational (Fig. 4F). Near the contact, arkosic paragneiss outcrops contain centimeter-scale alternating bands of feldspar- and quartz-rich layers (Figs. 4D and 5). Over ~3 m of structural section, layers of calc-silicate paragneiss become thinner and less abundant relative to layers of arkosic paragneiss. The grain size also changes, with fine pebbles and coarse sand grains in the arkosic paragneiss and fine sand- to silt-size grains in the calc-silicate. Seen in thin section, the transition from arkosic to calc-silicate paragneiss includes the addition of clinopyroxene, epidote, and titanite. Penetrative strain along the contact is relatively low. The contact appears to be premetamorphic and is interpreted to be originally depositional, although we cannot rule out premetamorphic brittle faulting.

The field and petrographic data suggest that the protoliths of the YAC paragneiss unit include arkosic sandstone and local fine-pebble conglomerate (arkosic paragneiss), quartz arenite (quartzite), calcareous siltstone and mudstone (calc-silicate paragneiss), and marble. Together with plutonic-derived clasts and abundant zircon (see following) these units are interpreted to represent a shallow-marine sequence fringing a continental margin magmatic arc.

Orthogneiss

At Yellow Aster Meadows and Kidney Creek (Figs. 2, 3), coarse grained quartz-feldspar augen gneiss is compositionally homogeneous on the scale of tens of meters along and across strike of the foliation and is interpreted as orthogneiss. Abundant pale green altered plagioclase and centimeter-scale K-feldspar augen are characteristic of this lithology (Figs. 6A–6D), but some

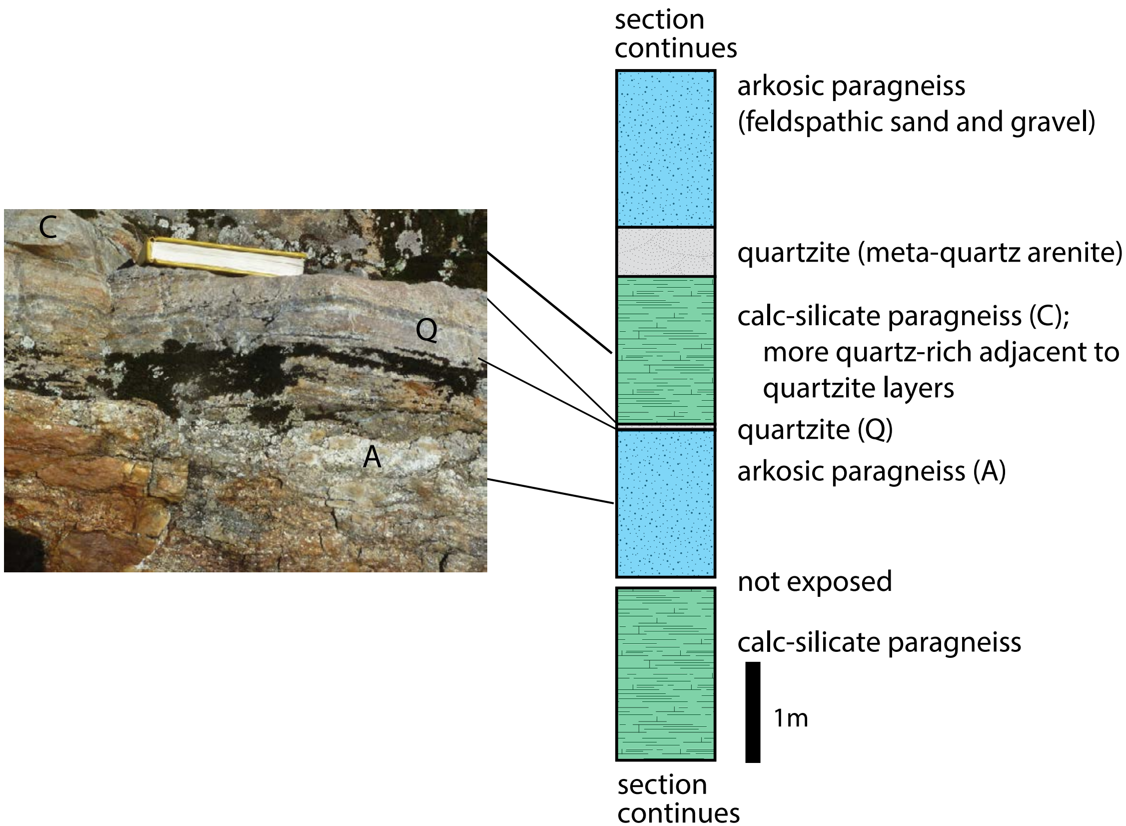

Figure 5. Details of contact between calc-silicate paragneiss and arkosic paragneiss at Yellow Aster Meadows. (A) Photograph of a portion of area illustrated in B. (B) Lithologic column.

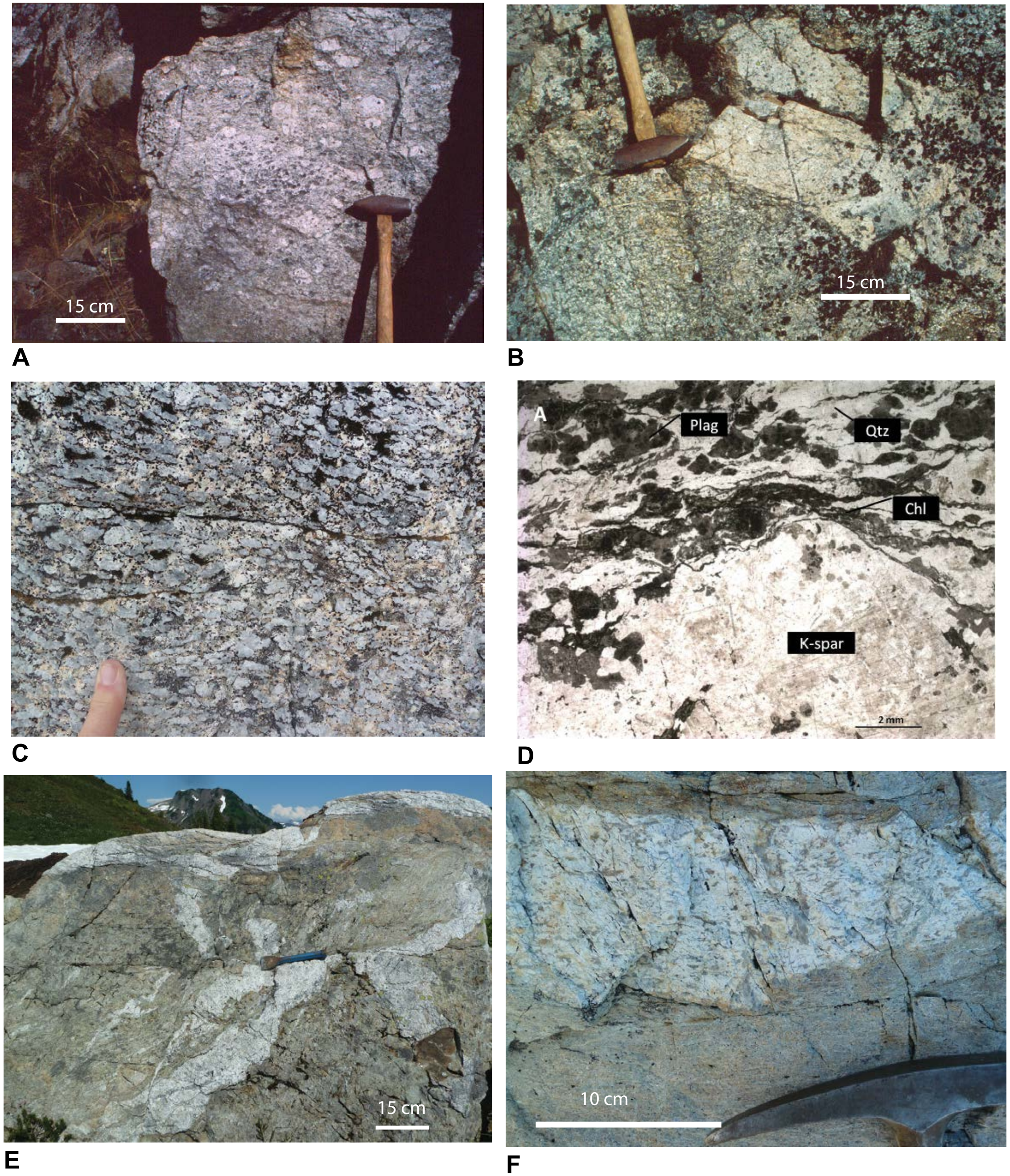

Figure 6. Photos of Yellow Aster Complex (YAC) igneous samples. (A) Augen gneiss sample 91–457. (B) Felsic dike (sample 91–458) cuts augen gneiss. (C) Augen gneiss sample 14YA21. (D) Photomicrograph of undated sample of augen gneiss, plane polarized light. Plag—plagioclase; Qtz—quartz; Chl—chlorite; K-spar—potassium feldspar. (E) Boudinaged syn-tectonic dikes crosscutting calc-silicate paragneiss; sample 14YA11 collected from lower right. (F) Weak foliation in syn-tectonic dike is parallel to foliation in calc-silicate paragneiss, near sample EAH34.

outcrops do not display K-feldspar augen. Contacts between K-feldspar-rich and poor rock types were not found, and major and trace-element geochemistry of the two varieties are very similar, with a granite composition (Kirkham, 2015). Quartz diorite has been reported by prior workers (Mattinson, 1972). In the granite gneiss, feldspar augen occur in a matrix of quartz (35%), plagioclase (25%–30%), K-feldspar (15%–20%), chlorite (5%–10%), and muscovite (5%) with minor epidote and calcite. A weak to moderate foliation is defined by layers of coarse-grained quartz and plagioclase with mylonitic chlorite. Foliation wraps euhedral K-feldspar phenocrysts (Fig. 6D). Coarse-grained quartz occurs as ribbons with undulose extinction. The relationship between the orthogneiss and paragneiss is uncertain. Calc-silicate paragneiss crops out adjacent to orthogneiss east of Yellow Aster Butte (Fig. 3), and occurs as float within the area of mapped orthogneiss, but the contact was never observed and is locally marked by serpentinite, suggesting overprinting during later faulting.

Coarse-grained mafic orthogneiss is locally observed to intrude the paragneiss. Compositional layering in this unit suggests a protolith of layered gabbro; the compositional layering is folded and crosscut by metamorphic foliation.

Weakly foliated leucogranite gneiss (quartz-feldspar-muscovite ± biotite) crosscuts the paragneiss (Figs. 6E, 6F). Intrusions that crosscut foliation at a low angle also contain foliation parallel to that in the wall rock and are boudinaged in the foliation plane, suggesting syn-tectonic intrusion (Figs. 6E, 6F). Although similar appearance, mineral content, and weak foliation suggest that these dikes and irregular intrusions may be related to the granitic orthogneiss, differences in chemistry and Hf isotopes (see following) do not support that hypothesis.

Post-Tectonic Intrusions

Felsic and mafic igneous rocks intrude both paragneiss and orthogneiss. Decameter-scale irregular bodies of fine- to medium-grained and porphyritic tonalite, diorite, and gabbro appear to predate fine-grained to aphanitic dikes. These intrusions appear to postdate ductile deformation and high-grade metamorphism based on fragmented and foliated wall rock preserved within the intrusions and observed crosscutting relationships. Post-tectonic intrusions were sampled, but with the exception of one sample (91–458, Fig. 6B), did not yield zircon for U-Pb dating.

Sample Descriptions

We collected 11 samples of paragneiss from Schreibers Meadow and Yellow Aster Meadows. At Schreibers Meadow (Fig. 2), samples were collected from large blocks in a boulder field below cliff outcrops of paragneiss intruded by post-tectonic intrusions. Compositional variation and crosscutting relations are more easily observed in the fresh blocks than in the cliff face. Samples EAH10b and EAH11 consist of quartzose calc-silicate paragneiss that occurs intercalated with marble and intruded by mafic and felsic dikes (Fig. 4B). Sample 14YA1 is quartzose calc-silicate paragneiss that is intruded by the post-tectonic leucocratic intrusion dated in Brown et al. (2010) as 418 Ma. Sample EAH03 is a pyroxene calc-silicate paragneiss with no compositional layering. In the field we originally interpreted EAH03 as an orthogneiss due to its homogeneous appearance over several meters, and analyzed it as an igneous sample. Sample YA5 is a calc-silicate paragneiss collected from a roadcut ~2 km southeast of Schreibers Meadow (Fig. 2). At Yellow Aster Meadows, samples of arkosic paragneiss include 91–456, 13YA1, and 14YA28 (Fig. 3). These samples contain centimeter-thick compositional layering defined by differing quartz and feldspar abundance, as well as different grain size (Fig. 4). Quartzose calc-silicate paragneiss samples 14YA15 and EAH39 were collected a few meters structurally below samples 91–456 and 13YA1, respectively; sample 14YA19 was collected from another fault block of quartzose calc-silicate paragneiss (Figs. 3 and 4). Arkosic paragneiss samples predominantly contain medium to coarse sand-size relict quartz and feldspar grains with as much as 10% fine pebbles. Calc-silicate paragneiss samples are finer grained, with silt and fine sand-size relict quartz grains.

Six samples of orthogneiss and dikes were collected from the YAC. Orthogneiss samples 14YA21 and 14YA27 are coarse-grained granitic gneiss at Yellow Aster Meadows (Figs. 3 and 6C). Sample 91–457 is a felsic augen orthogneiss collected in the Kidney Creek block, where it is cut by unfoliated dike sample 91–458 (Figs. 6A, 6B). Samples EAH34 and 14YA11 are weakly foliated leucogranite dikes that crosscut the calc-silicate paragneiss of sample 14YA19 (Figs. 3, 6E, and 6F).

METHODS

Zircon separation was done at Western Washington University and the Arizona LaserChron Center using standard sample preparation (Gehrels et al., 2000, 2008; Gehrels and Pecha, 2014). U-Pb geochronology of zircons was conducted by laser ablation–multicollector inductively coupled plasma–mass spectrometry (LA-MC-ICP-MS) at the Arizona LaserChron Center (Gehrels et al., 2006, 2008; Gehrels and Pecha, 2014). Sri Lanka, FC-1, and R33 zircon crystals are used as primary standards.

Mass spectrometry analysis for this study was conducted in multiple sessions. For U-Pb geochronology analyses prior to 2014 (EAH samples and YA5), ~100 detrital zircons and 25 magmatic zircons were analyzed with a spot diameter of 30 µm. In 2014–2015 sessions (samples prefaced by 13YA, 14YA, and 91–), analysis of 400 detrital zircons and 50 magmatic zircons was done for samples with sufficient zircon, and the spot size was 20 µm. For detrital zircon analyses, cathodoluminescence (CL) and backscatter electron images were used to select grains randomly, only avoiding grains that were too small or that had cracks or inclusions. In the detrital zircon samples most grains have very thin unzoned rims, interpreted as metamorphic (Supplemental Fig. S1[1]). Where

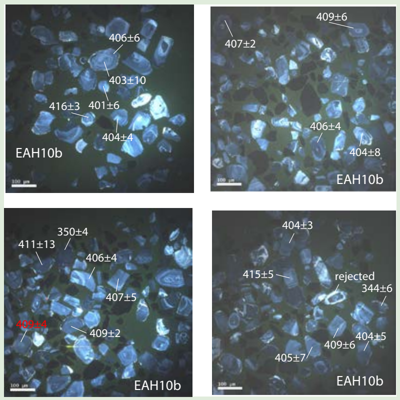

[1]Supplemental Files. Figure S1: Cathodoluminescence backscatter electron images for selected detrital zircon samples. Figure S2: Cathodoluminescence images for orthogneiss sample 14YA27. Table S1: U-Pb data and sample location information. Table S2: Hf data. Please visit http://doi.org/10.1130/GES01557.S1 or the full-text article on www.gsapubs.org to view the Supplemental Files.

an igneous core (e.g., a prismatic grain with growth zoning) was surrounded by a metamorphic (e.g., rounded and/or unzoned) rim, we analyzed the core. In grains with apparent xenocrystic igneous cores and texturally distinct igneous rims, we analyzed the outer igneous part if it was large enough. For igneous samples, we targeted prismatic grains with no inclusions and growth zoning evident on CL images. Grains where both core and rim were analyzed are indicated in Table S1 (footnote 1) by C and R, respectively. Example CL images are shown in Figures S1 and S2 (footnote 1).

U-Pb analytical data are reported in Table S1 (footnote 1). Uncertainties shown in these tables are at the 1σ level, and include only measurement errors. For ages older than 600 Ma, analyses that are >20% discordant (by comparison of $^{206}Pb/^{238}U$ and $^{206}Pb/^{207}Pb$ ages) or >5% reverse discordant are not considered further, and are typically not listed in Table S1. For ages younger than 600 Ma, where discordance cannot be accurately calculated due to the imprecision of the $^{206}Pb/^{207}Pb$ age (Gehrels et al., 2008), we used a 40% discordance cutoff. Discordant grains are shown by strikeout in Table S1. The Best Age column is determined from $^{206}Pb/^{238}U$ age for analyses with $^{206}Pb/^{238}U$ ages younger than 900 Ma and from $^{206}Pb/^{207}Pb$ age for analyses with $^{206}Pb/^{238}U$ ages older than 900 Ma.

The resulting interpreted ages are shown on Pb*/U concordia diagrams and relative age-probability diagrams using the routines in Isoplot (Ludwig, 2008) (Table S1). The age-probability diagrams show each age and its uncertainty (for measurement error only) as a normal distribution, and sum all ages from a sample into a single curve. For detrital samples, composite age probability plots are made from an in-house Excel program that normalizes each curve according to the number of constituent analyses, such that each curve contains the same area, and then stacks the probability curves. For igneous samples and analysis of the maximum depositional age of detrital samples, the weighted mean diagrams show the weighted mean (weighting according to the square of the internal uncertainties), the uncertainty of the weighted mean, the external (systematic) uncertainty that corresponds to the ages used, the final uncertainty of the age (determined by quadratic addition of the weighted mean and external uncertainties), and the MSWD (mean square of weighted deviates) of the data set. Age peaks shown on probability diagrams and discussed in text were calculated using the Unmix routine in Isoplot (Ludwig, 2008) and the in-house Age Pick program.

Hf isotope analyses were conducted with a Nu HR (high resolution) ICP-MS connected to a Photon Machines Analyte G2 excimer laser. Seven different standard zircons (Mud Tank, 91500, Temora, R33, FC52, Plesovice, and Sri Lanka) were analyzed with unknowns on the same epoxy mounts. Laser ablation analyses were conducted with a laser beam diameter of 40 µm, with the ablation pits located on top of the U-Pb analysis pits. CL images were used to ensure that the ablation pits do not overlap multiple age domains or inclusions. Zircons for Hf analyses were selected to include the major age groups identified from the U-Pb dating. Hf isotopic composition is monitored during each analysis. Any analyses that show a downhole change in Hf isotopic composition were rejected. This helps eliminate analyses that are compromised by ablation of multiple age domains.

The $^{176}Hf/^{177}Hf$ at time of crystallization is calculated from measurement of present-day $^{176}Hf/^{177}Hf$ and $^{176}Lu/^{177}Hf$, using the decay constant of ^{176}Lu ($\lambda = 1.867e^{-11}$) from Söderlund et al. (2004). Depleted mantle model ages are not calculated because the $^{176}Hf/^{177}Hf$ and $^{176}Lu/^{177}Hf$ of the source materials from which the zircon crystallized are not known.

U-Pb AND Hf RESULTS

Detrital Zircon Samples

We chose three samples of arkosic paragneiss and eight samples of quartzose calc-silicate paragneiss for geochronologic analysis. Zircons in the paragneisses range from <20 to ~150 µm; calc-silicate paragneiss samples are finer grained than the arkosic paragneiss, typically yielding fewer zircons large enough for both U-Pb and Hf analyses. Results are reported in Figures 7 and 8 and Tables S1 and S2 (footnote 1). Analyses are predominantly from individual zircon grains, with relatively few core and rim analyses (Table S1; Fig. S1; see footnote 1).

Arkosic Paragneiss

Sample 13YA1 yielded 267 U-Pb analyses and 118 Hf analyses. The youngest age peak is at 414 Ma, and prominent peaks occur at 1900–1800 Ma and 2567 Ma within a broad assemblage of grains from 2700 to 1000 Ma (Fig. 7). The $\varepsilon Hf_{(t)}$ values of the Paleozoic grains range from –20 to –57 (Fig. 8). Hf isotopes of Precambrian grains form two populations, with a cluster of 1700–1000 Ma grains with positive $\varepsilon Hf_{(t)}$ and a spread of late Neoproterozoic to Archean grains along a crustal evolution curve that intersects the depleted mantle curve at 3.0 Ga (Fig. 8).

Sample 91–456 yielded 264 U-Pb and 57 Hf analyses. The youngest age peak is at 408 Ma. Precambrian grains yield a series of small peaks from 2700 to 1000 Ma, with the largest peak at 1880–1840 Ma and subsidiary peaks at 1658 and ca. 2570 Ma (Fig. 7). The $\varepsilon Hf_{(t)}$ values of Paleozoic grains range from –10 to –40, those of Proterozoic grains younger than 1800 Ma are predominantly 0–10, and grains older than 1800 Ma plot roughly along a crustal evolution curve extending back to before 3.0 Ga (Fig. 8).

Sample 14YA28 yielded 98 U-Pb analyses and 66 Hf analyses. The predominant age peak occurs at 402 Ma, with subsidiary peaks at 1900–1800 and ca. 2500 Ma and a series of smaller peaks in the age range from 3000 to 1000 Ma (Fig. 7). The $\varepsilon Hf_{(t)}$ values for Devonian grains range from –5 to –15, and Proterozoic and Archean grains form two populations, with 1800–1000 Ma grains having predominantly positive $\varepsilon Hf_{(t)}$ values [$\varepsilon Hf_{(t)}$ +2 to +10] and older grains plotting along a 3.0 Ga crustal evolution curve with the other arkosic samples (Fig. 8).

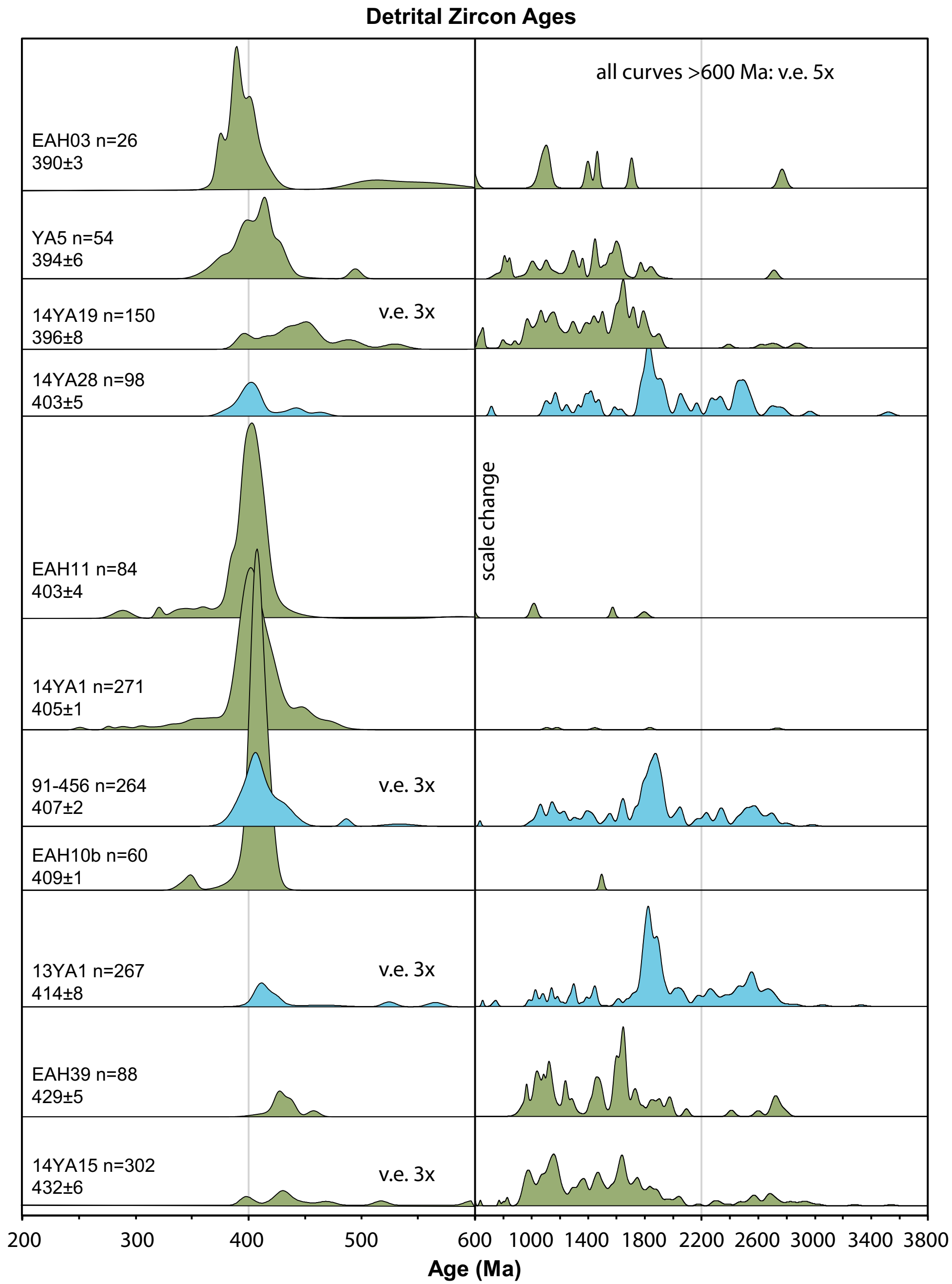

Figure 7. Normalized probability plots showing U-Pb ages for Yellow Aster Complex (YAC) paragneiss samples. See Table S1 (footnote 1) for data and additional plots. Plots are ordered by maximum depositional age, calculated as described in text, with inferred age indicated beneath sample number. Blue curves are for arkosic paragneiss, green curves are for calc-silicate paragneiss. Note X-axis scale change at 600 Ma. Some curves shown with vertical exaggeration (v.e.) for clarity.

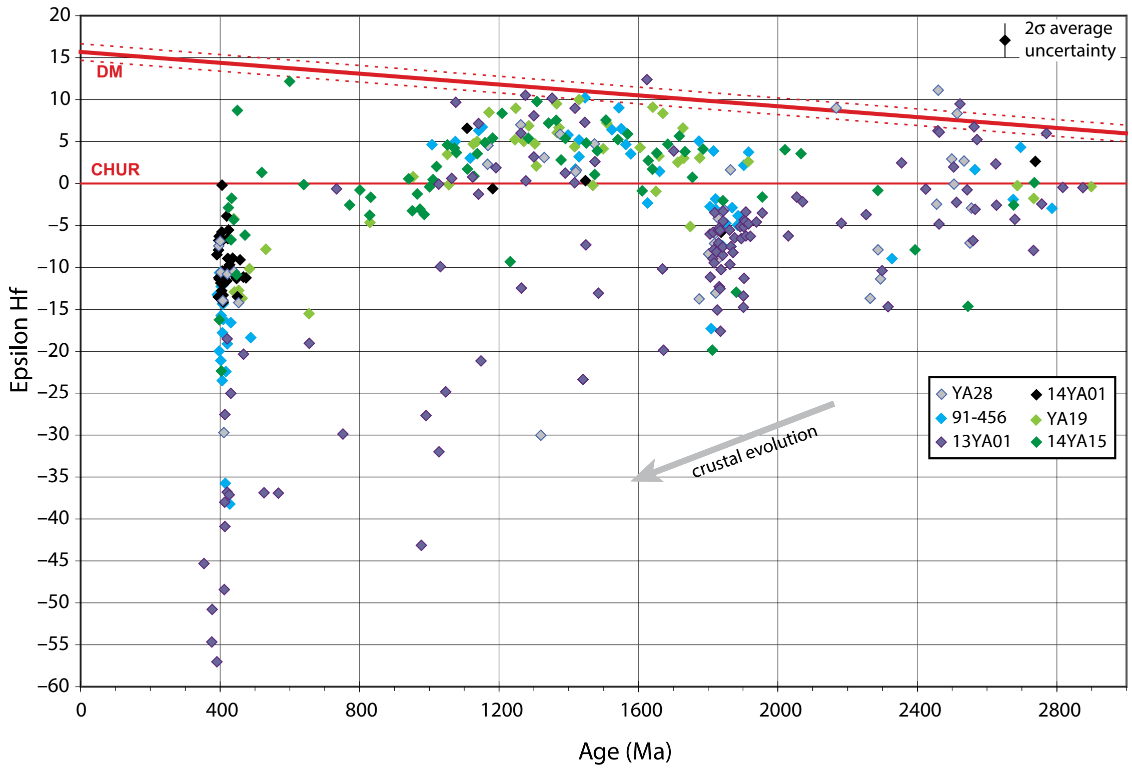

Figure 8. Hf isotope data for Yellow Aster Complex paragneiss samples. Arkosic paragneiss samples are 91–456, 14YA28, 13YA1; calc-silicate paragneiss samples are 14YA15, 14YA19, 14YA1. DM—depleted mantle (Vervoort and Blichert-Toft, 1999); CHUR—chondritic uniform reservoir (Bouvier et al., 2008); gray arrow shows slope of average crustal evolution assuming present-day $^{176}Lu/^{177}Hf$ = 0.0115 (Vervoort and Patchett, 1996; Vervoort et al., 1999). Data are in Table S2 (see footnote 1).

Calc-Silicate Paragneiss

Samples analyzed for U-Pb (but not Hf; Hoffnagle, 2014) include four samples from Schrieber's Meadow (EAH03, EAH10b, EAH11, YA5) and one from Yellow Aster Meadows (EAH39). Samples EAH03 (n = 26), EAH10b (n = 60), and EAH11 (n = 84) contain predominantly Devonian grains, with age peaks at 390 Ma, 409 Ma, and 403 Ma, respectively, together with a small number of Precambrian grains (Fig. 7). In sample YA5 (n = 54), approximately half the grains are Precambrian, scattered from 2000 to 1000 Ma; Paleozoic grains range from 420 to 360 Ma and form peaks ca. 417 and 394 Ma (Fig. 7). In contrast, sample EAH39 (n = 88) contains abundant Precambrian grains forming a broad set of peaks between 2000 and 1000 Ma and relatively fewer Paleozoic grains with a poorly defined peak at 429 Ma (Fig. 7).

Calc-silicate paragneiss samples analyzed for both U-Pb and Hf include 14YA1 from Schreibers Meadows, and 14YA15 and 14YA19 from Yellow Aster Meadows. Sample 14YA1 yielded 271 U-Pb analyses and 43 Hf analyses. U-Pb ages are strongly clustered at 405 Ma (Fig. 7). The $\varepsilon Hf_{(t)}$ for the Paleozoic grains ranges from ~0 to –14 (Fig. 8). Sample 14YA15 yielded 302 analyses and 66 Hf analyses. Paleozoic grains are relatively sparse and the youngest peak composed of ≥3 grains is ca. 432 Ma; Precambrian grains form peaks at 984, 1164 Ma, 1642, and 1754 Ma and a lower set of peaks between 3000 and 2300 Ma (Fig. 7). The $\varepsilon Hf_{(t)}$ values of the Paleozoic grains range from +9 to –22 while $\varepsilon Hf_{(t)}$ for the Precambrian grains are dominantly positive, ranging from ~+10 to –5 (Fig. 8). Sample 14YA19 yielded 150 U-Pb and 41 Hf analyses. The probability plot resembles that of samples 14YA15 and EAH39 for the Precambrian grains, but the Paleozoic grains show peaks with ≥3 grains at 453 and 396 Ma (Fig. 7; Table S1; footnote 1). The $\varepsilon Hf_{(t)}$ values of the Paleozoic grains (n = 6) range from –4 to –14, while Precambrian grains range from –5 to +9 (Fig. 8).

Igneous Samples

Orthogneiss

The three orthogneiss samples contain a mix of Ordovician to Devonian zircons ranging in size from ~50 to 200 μm; age interpretations are complicated by evidence of both inheritance and Pb loss, and an inability to resolve discordance for these populations. After discarding anomalously high-U grains in samples that contain distinct populations of lower U and higher U grains, using the Unmix routine in Isoplot (Ludwig, 2008), and calculating the weighted mean age of the youngest population, the age of each sample was estimated. Orthogneiss samples 14YA21, 14YA27, and 91–457 have weighted mean ages of ca. 407, ca. 410, and ca. 406 Ma, respectively (Fig. 9). However, 14YA21 also contains a population of ca. 395 Ma zircons that is neither substantially higher in U content than the older population (Table S1; footnote 1) nor visually distinct from it. Two of the samples contain significant populations of ca. 460–440 Ma grains that are not identifiable as distinct in CL images (Fig. 9; Fig. S2; see footnote 1). The $\varepsilon Hf_{(t)}$ values for all three orthogneiss samples cluster tightly between 0 and –6 (Fig. 10).

Dikes

Two samples of syn-tectonic felsic dikes were analyzed. Samples 14YA11 and EAH34 appear to crosscut foliation in the paragneiss at a low angle but also are weakly deformed. Both samples yield abundant Precambrian zircons and few Paleozoic grains; grain sizes are typically <100 µm. In sample 14YA11, a selection of 7 Paleozoic grains form a linear array on the Tera-Wasserburg plot yielding an approximate age of 410 Ma (Fig. 9). Sample EAH34 did not contain enough Paleozoic ages to determine an emplacement age, but the youngest single grain is 406 ± 8 Ma (Table S1 [footnote 1]). Hf analysis of sample 14YA11 (Fig. 10) shows Paleozoic grains with $\varepsilon Hf_{(t)}$ values of –5 to –27, and negative values on the Precambrian grains that are similar to those of the calc-silicate

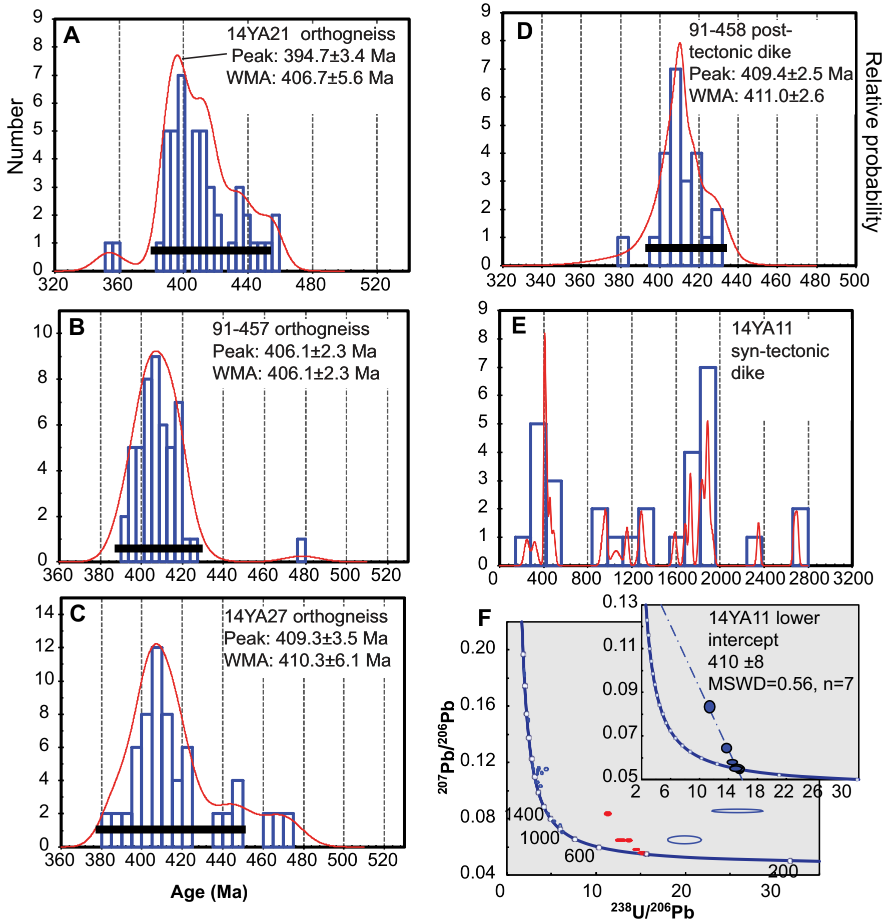

Figure 9. (A–E) Histograms and probability plots for Yellow Aster Complex igneous samples. Peak age is calculated weighted mean average of grains in youngest peak with >3 grains, as determined by AgePick software. WMA—weighted mean age of grains (black bar). (F) Age for sample 14YA11 is calculated from regression of red points on Tera-Wasserburg plot in lower right. MSWD—mean square of weighted deviates. See Table S1 (footnote 1) for data and additional plots.

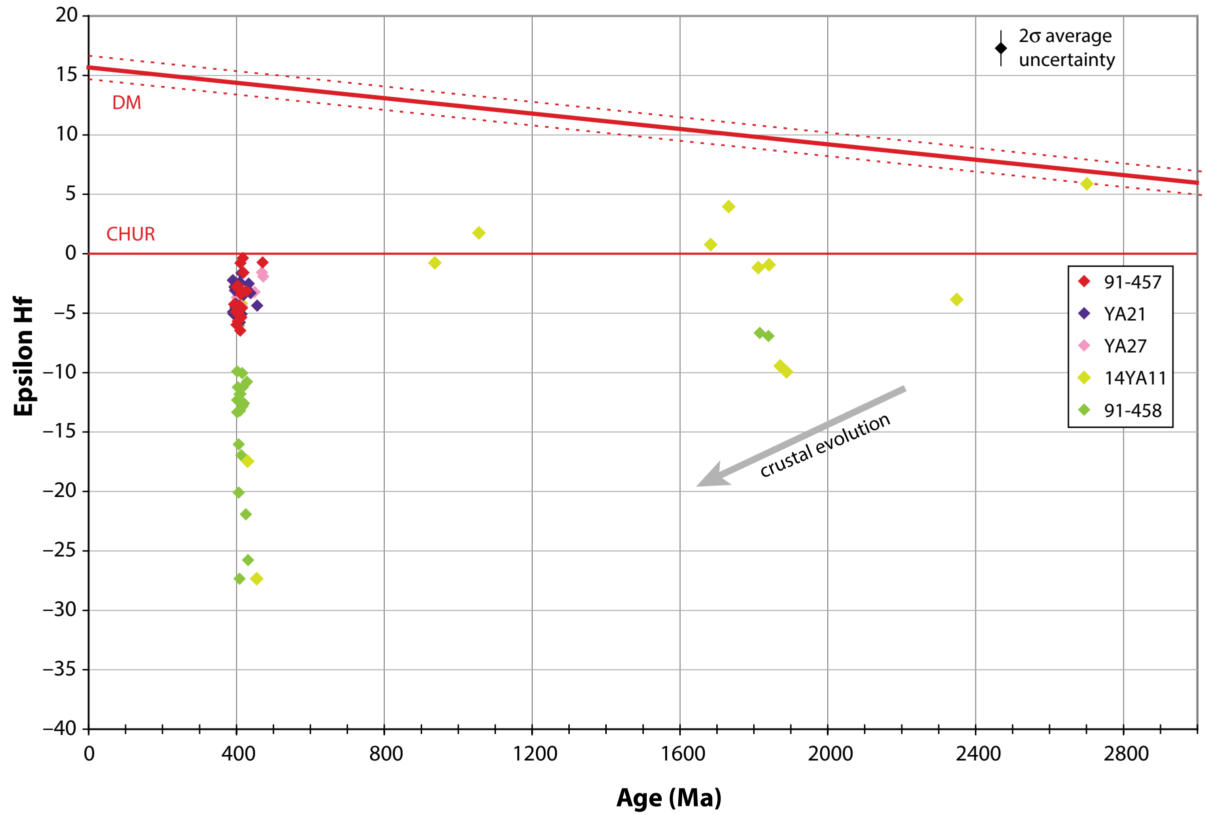

Figure 10. Hf isotope data for Yellow Aster Complex (YAC) igneous samples. Samples 14YA21, 14YA27, and 91–456 are orthogneiss; samples 14YA11 and 91–458 are dikes. Data are in Table S2 (see footnote 1). DM—depleted mantle; CHUR—chondritic uniform reservoir.

paragneiss it intrudes (represented by sample 14YA19). We suspect that the majority of grains in both dike samples are inherited from the wall-rock paragneiss, thus it is difficult to establish a precise intrusion age; both dikes are likely younger than ca. 410 Ma.

One post-tectonic dike sample yielded zircon. The youngest population in sample 91–458 is 409.2 ± 2.5 Ma and its weighted mean age is 411.0 ± 2.6 Ma (Fig. 9). Cores of several Paleozoic zircons range from 2086 to 1815 Ma. This dike crosscuts the orthogneiss of sample 91–457 (406 ± 2 Ma) (Fig. 6B). The weighted mean age of the dike is older than the age of the rock it crosscuts, suggesting a component of inheritance in the dike, and the age is likely younger than ca. 409 Ma. The combination of geologic and geochronologic data is consistent with the ages overlapping ca. 408–407 Ma. Hf analysis of dike sample 91–458 yields a range of values from –5 to –27 for the Paleozoic grains (Fig. 10).

INTERPRETATION

Depositional Ages of Paragneiss Protolith

There are no fossils in the YAC, so we use detrital zircon ages and crosscutting relations with plutonic rocks to infer the stratigraphic age of the paragneiss protolith. We calculated the maximum depositional age (MDA) of each paragneiss sample using the in-house AgePick procedure and MDA guidelines (www.laserchron.org) and the Unmix routine in Isoplot (Ludwig, 2008) for the youngest peak containing 3 or more grains with ages within 2σ error of each other (Dickinson and Gehrels, 2009) (histograms in Table S1; see footnote 1). In an attempt to eliminate zircons that might have undergone Pb loss during metamorphism, for the MDA analysis we also plotted U concentration versus age and eliminated the youngest grains in a sample that show an inverse relationship between U and age (these grains are shown on the probability plots). The youngest grains in some samples (14YA28, 91–456, 13YA1), and a few grains of a variety of ages in most samples have U/Th ratios >15, a possible indication that they are metamorphic zircons. However, the wide age range of these zircons, and the fact that they have sizes, shapes, and textures similar to igneous zircons on CL images (Fig. S1; see footnote 1) suggests that these are detrital grains, not in situ metamorphic zircons (Fig. 11). For example, in EAH11 and 14YA28, the metamorphic zircons are similar in grain size range and roundness to igneous ones (Fig. S1C; see footnote 1). Maximum depositional ages range from 409 ± 1 to 390 ± 3 Ma for the Schreibers Meadows samples, and 432 ± 6 to 396 ± 8 Ma for the Yellow Aster Meadows samples (Fig. 7). Owing to the apparently wide age range of Paleozoic zircons in the source area, combined with the difficulty of detecting Pb loss in individual grains of this age, we can only approximate the MDA of most samples. Nonetheless, the ages suggest Silurian to Early Devonian deposition, an interpretation consistent with previous ages of ca. 418–300 Ma for crosscutting intrusive rocks (Mattinson, 1972; Rasbury and Walker, 1992; Brown et al., 2010). The narrow age range of zircons in calc-silicate paragneiss samples such as EAH10b, EAH11, and 14YA1, the presence of very few inherited grains, and the observation of abundant fine euhedral zircons in these samples suggest a tuffaceous component in the sediments, indicating proximity to an active arc ca. 400 Ma.

We collected two sets of samples at Yellow Aster Meadows that appear to be in stratigraphic succession, a hypothesis that can be tested using the apparent maximum depositional ages. The northern sequence, in order from structurally low to high, includes EAH39 (MDA 429 ± 5 Ma), 13YA1 (MDA 414 ± 8 Ma), and 14YA28 (MDA 403 ± 5 Ma). The southern sequence includes 14YA15 (MDA 432 ± 6 Ma) and 91–456 (MDA 407 ± 2 Ma) (Figs. 3 and 7). Maximum depositional ages appear to be consistent with this sequence being upright, but possibly span a much longer period of time than the actual sedimentation, because the thickness perpendicular to the foliation is only ~10 m and there is a possibility that, given the small number and fine grain size of grains in the arkosic unit, we did not analyze the youngest grains. The possibility that there is an unconformity between the two types of paragneiss is unlikely because neither the calc-silicate nor arkose ages are consistently younger than the other (Fig. 7).

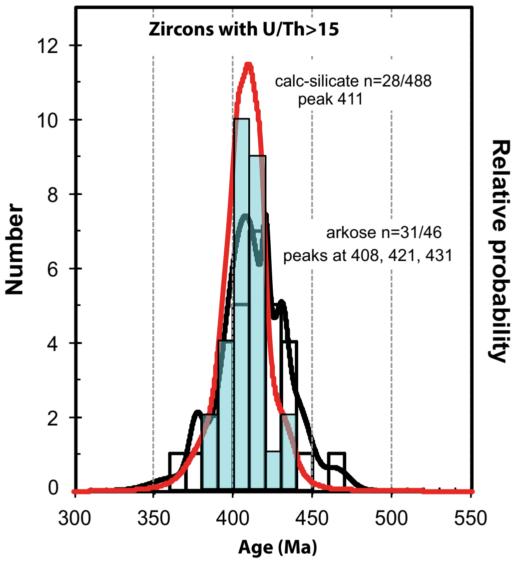

Figure 11. Histogram and probability plot of Paleozoic zircons with U/Th > 15 from all detrital samples. Plotted grains may represent metamorphic grains (see text for discussion). Blue bars with red curve are for calc-silicate paragneiss, white bars with black curve are for arkosic paragneiss. Compare with larger populations in Figure 7.

Different Provenance of Two Paragneiss Protoliths

While all the paragneiss samples show evidence of a combined provenance of Precambrian craton and Ordovician to Early Devonian arc rocks, the U-Pb age patterns and the Hf isotope data suggest that the arkosic paragneiss and the calc-silicate paragneiss were derived predominantly from different sources. Precambrian grains in the calc-silicate paragneiss show a broad peak from 2000 to 900 Ma and a small peak ca. 2700 Ma, while those in arkosic paragneiss have a predominant peak at 1800 Ma, fewer grains in the range 1700–900 Ma, and several small peaks in the range 3000–2000 Ma (Fig. 7B). Hf isotopes are also distinct, with significantly more negative $\varepsilon Hf_{(t)}$ in the arkosic relative to the calc-silicate paragneiss, particularly in Paleozoic grains (Fig. 8). A significantly higher percentage of Paleozoic grains in the arkosic paragneiss are possibly metamorphic grains with U/Th > 15 (31/46) relative to the calc-silicate paragneiss (28/488), suggesting derivation from an early Paleozoic orogenic belt (Fig. 11). Both units contain abundant Ordovician–Early Devonian age detrital zircons with U/Th < 10, suggesting derivation from early Paleozoic arc terranes. In both types of paragneiss, Precambrian zircons occur as individual grains and as cores surrounded by Paleozoic zircon. However, the significantly more negative $\varepsilon Hf_{(t)}$ value in the arkosic paragneiss suggests that its protolith received detritus from a continental arc built on Archean crust, while at the same time, the calc-silicate protolith arc source was more juvenile or built on Proterozoic crust (Figs. 8 and 10). Because relict detrital quartz, feldspar, and lithic grains in the arkosic paragneiss are typically much coarser than in the calc-silicate paragneiss, we interpret a relatively proximal source. Despite field and petrographic similarities, there is a distinct difference between calc-silicate samples from Schreibers Meadows and those from Yellow Aster Meadows; the former contain predominantly Devonian zircons, with fewer Precambrian zircons, and the Devonian zircons are typically euhedral. The samples from Yellow Aster Meadows contain few Paleozoic grains relative to abundant Precambrian grains, and most grains are relatively rounded. We interpret the Schreibers Meadows calc-silicate protolith to represent a facies that was more proximal to the Devonian arc than the calc-silicate at Yellow Aster Meadows.

Age and Tectonic Setting of Deformation and Metamorphism

The metamorphic and deformational history of the YAC can be inferred from the combined age data and field relationships. Intrusions interpreted to be pre-tectonic (orthogneiss), syn-tectonic, and post-tectonic yield overlapping ages from ca. 410–406 Ma. Determination of the exact ages of events is problematic due to Pb loss and inheritance. However, dating of orthogneiss and a crosscutting dike from the same outcrops (samples 91–457, 91–458) that are within error of each other ca. 408–407 Ma suggests that one episode of deformation and metamorphism occurred at this time in the Early Devonian. An older (Ordovician) age of deformation and initiation of magmatism within the YAC was inferred by Brown et al. (2010) from their post-tectonic dike sample YA3, interpreted to be 418 Ma from the youngest population (n ≥3) of zircons in the sample. The maximum depositional age of sample 14YA1 (405 Ma), a sample of the wall rock cut by this dike, requires that the dike is younger and that the dated zircons in YA3, which range in age from 467 to 405 Ma (Brown et al., 2010), are all inherited from the wall rock. The presence of three populations of Paleozoic zircons, ca. 400, ca. 420, and ca. 450 Ma, in most of the samples (including igneous samples) suggests a long history of magmatism from before 450 to after 400 Ma within the YAC and within the source area of its sedimentary protoliths. The felsic composition of igneous rocks, trace element data (Kirkham, 2015), and the negative $\varepsilon Hf_{(t)}$ further suggest that arc magmatism occurred in a continental margin environment. The wide range of $\varepsilon Hf_{(t)}$ for Ordovician–Devonian grains, and the inheritance of Silurian and Ordovician zircons in Devonian magmas, suggests a period of recycling of older crustal constituents. The $\varepsilon Hf_{(t)}$ for zircons in the orthogneiss are higher than those of similar age zircons in samples of dikes and paragneisses, suggesting these plutons may have been emplaced in thinner or younger (Proterozoic) crust. However, we do not claim that our sampling of arc plutonic rocks is complete, and more work needs to be done on the post-tectonic plutonic suite.

DISCUSSION: ORIGIN OF THE YAC

Data from this study, when combined with previous work on similar early Paleozoic arc terranes in the North American Cordillera, yield insight into the origin and tectonic setting of the YAC and provide constraints on models for the accretion of far-traveled terranes to western North America. We evaluate the possible origin of the YAC by using our results to interpret the provenance of detrital zircons in the paragneisses and provide constraints on the possible location of early Paleozoic arc magmatism and deformation. We compare the lithologic and isotopic data to similar age rocks of parautochthonous western North America, to accreted peri-Laurentian terranes such as the Yukon-Tanana, and to exotic arc terranes such as the Alexander, Eastern Klamath, and Northern Sierra terranes (Fig. 1), all of which have been previously proposed to be similar to YAC and the related Chilliwack terrane (Miller, 1987; Rubin et al., 1990a; Gehrels et al., 1991; Mortensen, 1992; Brown et al., 2010; Hoffnagle, 2014). The combined U-Pb and Hf data provide an improved comparison tool for terrane correlation studies compared to the limited U-Pb data used in previous studies. Because the location of YAC as blocks in a Cretaceous mélange prevents us from using kinematic data to reconstruct the tectonic history, we use comparisons with other terranes to put the YAC in the context of previous models for Paleozoic–Mesozoic evolution of western North America. We conclude with a brief summary of constraints on current models for how the YAC became incorporated in the Northwest Cascades thrust system and was transported to its current location.

Gehrels et al. (1991) proposed, on the basis of similar lithology and ages, that the YAC and part of the Yukon-Tanana terrane in southeast Alaska were correlative. A peri-Laurentian affinity for the YAC and the composite Chilliwack terrane was supported by the observation (Brown et al., 2010) that U-Pb detrital zircons in the YAC are similar to the northern Cordilleran passive margin and the Yukon-Tanana terrane, and the interpretation that the quartz-rich sediment and marble indicate a passive margin setting for the YAC prior to arc magmatism, as also suggested for the Yukon-Tanana terrane. The U-Pb data (Brown et al., 2010) only limited the paragneiss age to between 1000 and 418 Ma, so permissive correlations were made with Cambrian–Ordovician passive margin rocks as a basement to an Ordovician–Devonian arc. However, Brown et al. (2010) noted that magmatism appeared to have begun earlier in the YAC than in the Yukon-Tanana terrane; Silurian arc magmatism is unknown in western Laurentia and thus they suggested that the Chilliwack terrane may have been connected to the Alexander terrane. Our U-Pb data require an Early Devonian age for most of the dated paragneiss samples, and the Hf data provide more basis for comparison with other terranes, thus we are able to reconsider and test the terrane correlations of Brown et al. (2010).

Peri-Laurentian and Non-Laurentian Precambrian Detrital Zircon Patterns

To assess which continental margin the YAC formed on, we compare Precambrian detrital zircon patterns of YAC samples to data from passive margin rocks of western Laurentia, the Arctic margin, Greenland, and Baltica for sedimentary rocks of Devonian and older age deposited on those margins, and to igneous rocks of the shield regions and magmatic arcs (Fig. 12). We consider possible separate sources for the arkosic and calc-silicate paragneisses given their distinct lithologic and isotopic characteristics. U-Pb age and Hf isotope patterns of detrital zircons in the YAC arkosic paragneiss are most similar to strata of the northern British Columbia passive margin (Gehrels and Pecha, 2014), including a predominant age peak at 1.9–1.8 Ga and a smaller peak at 2.7–2.5 Ga (Fig. 12). A major difference is the abundance of Ordovician–Devonian zircons, which are absent in passive margin strata older than Late Devonian. The age of basement provinces exposed in northwestern Laurentia is consistent with relatively local derivation of Paleoproterozoic and Archean detritus in the arkosic paragneiss (e.g., Gehrels and Pecha, 2014, and references cited therein).

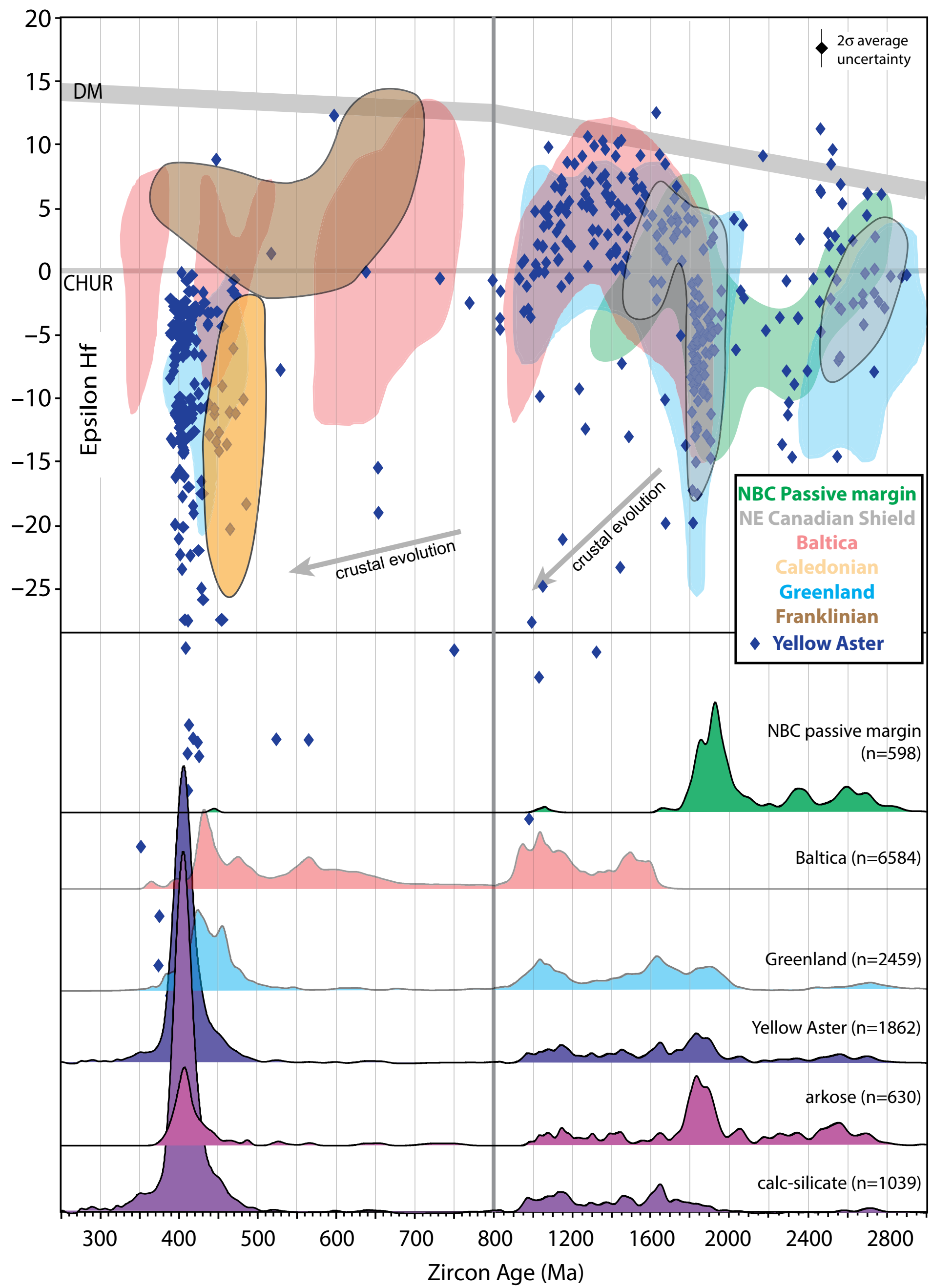

Figure 12. U-Pb and Hf data of samples from the Yellow Aster Complex compared with western Laurentia and other continental margins. The probability plot and Hf data labeled Yellow Aster includes both detrital and igneous zircons. Note change of X-axis scale at 800 Ma. DM—depleted mantle; CHUR—chondritic uniform reservoir. Gray arrows show slope of average crustal evolution as in Figure 8. Data sources: Northern British Columbia (NBC) passive margin detrital zircons: Gehrels and Pecha (2014). Baltica igneous and detrital zircons (older than 360 Ma): Andersen et al. (2002, 2007, 2011); Bingen and Solli (2009); Roberts et al. (2010); Brander et al. (2011); Corfu et al. (2011); Augland et al. (2012a, 2012b, 2014a, 2014b); Andresen et al. (2014); Gee et al. (2014); Kristoffersen et al. (2014); Lundmark et al. (2014); Slama and Pedersen (2015). Greenland igneous and detrital zircons (older than 360 Ma): Røhr et al. (2008); Kalsbeek et al. (2008); Rehnström (2010); Corfu and Hartz (2011); Slama et al. (2011); Augland et al. (2012a, 2012b); Andersen (2013). Canadian Shield Hf data: Stevenson and Patchett (1990). Franklinian Hf data: Anfinson et al. (2012). Caledonian plutons Hf data: Appleby et al. (2010); Flowerdew et al. (2009).

The broad array of 2.0–1.0 Ga U-Pb ages and the $\varepsilon Hf_{(t)}$ of these zircons in the calc-silicate paragneiss are unlike pre–Late Devonian strata of the northern Cordillera (Fig. 12), but are similar to Baltica, Greenland, and the northeast Canadian Shield, including a significant (11% of Precambrian grains) population of grains within the 1.61–1.49 North American magmatic gap (NAMG) of Van Schmus et al. (1993). A possible source of the abundant Mesoproterozoic zircons in the calc-silicate paragneiss exists in the 1.2–1.0 Ga Grenville orogen of eastern North America (Fig. 13). The continuous array of 1.8–0.9 Ga grains is likely derived from the Sveconorwegian belt of southern Scandinavia and its reworking into Caledonian nappes (Bingen and Solli, 2009). Grains of this age are mostly absent from Early Devonian and older strata in British Columbia, but are abundant in passive margin strata of eastern Alaska, where they are inferred to have been sourced from a landmass offshore of northern Laurentia (Gehrels and Pecha, 2014). Upper Devonian and younger passive margin strata typically contain Mesoproterozoic zircons, suggesting a source of these grains was available on the western margin by that time (Gehrels and Pecha, 2014).

Similarities between the detrital zircon patterns of Devonian sedimentary rocks and Precambrian basement do not require that basement to be a direct source of detritus. Various models have been proposed to explain the occurrence of Grenville-aged detrital zircons in the western Laurentian passive margin. The Grenville clastic wedge formerly covered much of the North American craton and large transcontinental river systems delivered sediment of this age to the southwestern U.S. margin throughout Mesoproterozoic, Neoproterozoic, and early Paleozoic time (Rainbird et al., 1992, 2012). Neoproterozoic and Cambrian strata of northern Canada contain a broad peak of 1.5–1.0 Ga grains interpreted as originating from the Grenville clastic wedge, and younger autochthonous strata with this same population are interpreted to record recycling of Neoproterozoic rocks rather than erosion of Grenvillian basement rocks (Hadlari et al., 2012). The source of these rocks, in the Mackenzie Mountains (Fig. 13) (Hadlari et al., 2012, 2015), could also be the source of the Precambrian population of grains in calc-silicate paragneiss in the YAC, rather than being more proximal to currently exposed Grenville-aged rocks. NAMG-age grains could be recycled from Belt Supergroup strata in southern British Columbia and the northwestern U.S. (Ross and Villeneuve, 2003), but the absence of this population in nearby passive margin strata of southern British Columbia (Gehrels and Pecha, 2014) argues against that interpretation.

Sources of Early Paleozoic Zircon and Constraints on the Tectonic Setting of the YAC

Unlike YAC paragneisses, passive margin strata of western Laurentia contain no Paleozoic detrital zircons until after Middle Devonian time (Gehrels and Pecha, 2014). The abundance of Ordovician to Early Devonian detrital zircons in our samples suggests proximity to an arc that initiated before ca. 410 Ma, and the ages of orthogneiss and dikes indicate that the YAC was fully within a continental margin magmatic arc setting by ca. 410 Ma. Although populations

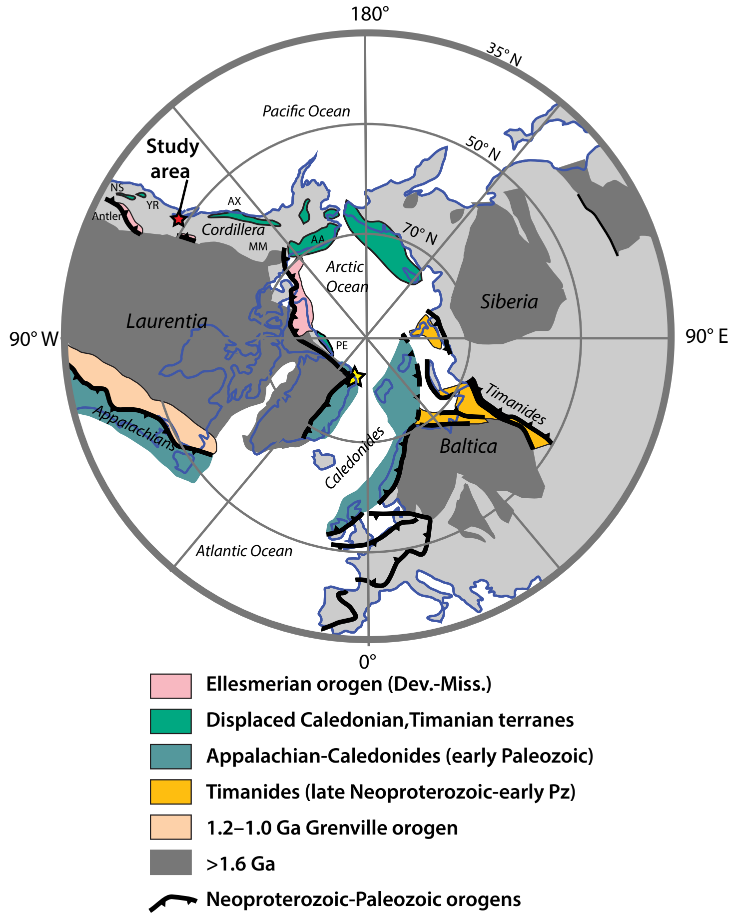

Figure 13. Simplified map of Precambrian cratons and Paleozoic orogenic belts for circum-Arctic continents (modified from Colpron and Nelson, 2011). Displaced Caledonian terranes that have geologic history similar to that of the Yellow Aster Complex (YAC) are labeled: NS—Northern Sierra, YR—Yreka, AX—Alexander, AA—Arctic Alaska, PE—Pearya, MM—Mackenzie Mountains. Red star indicates the study area; yellow star indicates our preferred site of origin of the YAC. Dev.-Miss.—Devonian–Mississippian; Pz.—Paleozoic.

of late Neoproterozoic to Early Devonian zircons in Late Devonian passive margin strata have been dated by U-Pb (Gehrels and Pecha, 2014), Hf isotope data on these grains are extremely sparse. Three Early Devonian grains analyzed by Beranek et al. (2016), show $\varepsilon Hf_{(t)}$ of −10 to −27. Data from Carboniferous and younger strata yield early Paleozoic zircons with $\varepsilon Hf_{(t)}$ values that are predominantly positive, but range from ~+15 to −15 (Gehrels and Pecha, 2014). These data suggest that sources of early Paleozoic zircon were not adjacent to western Laurentia until Late Devonian time. We infer that the Early Devonian detrital zircons in the YAC are derived from local igneous sources due to the abundance of dikes and orthogneiss of appropriate ages; however, the origin of Ordovician–Silurian zircons remains problematic.

We can consider the possibility that an arc developed off western Laurentia 40–50 m.y. earlier than inferred by previous workers (Late Devonian, ca. 360 Ma; e.g., Nelson et al., 2006), or the alternative, that the arc is exotic to western Laurentia (e.g., Gehrels et al., 1996; Harms et al., 2003; Wright and Wyld, 2006; Colpron and Nelson, 2009, 2011; Miller et al., 2011; Beranek et al., 2013a, 2013b; White et al., 2016). The comparison of Hf isotopes with known continental arcs of early Paleozoic orogens, including the Caledonides and Appalachians (Figs. 13 and 14), reveals that for YAC samples the Hf values of Ordovician to Early Devonian zircons overlap with Caledonian igneous rocks but extend to more negative $\varepsilon Hf_{(t)}$ values and include younger grains. Examination of Figure 12 suggests that while the U-Pb age pattern of the YAC data set is similar to both Greenland and Baltica, there is a greater proportion of Archean and Devonian grains and a lack of Neoproterozoic grains in the YAC. These observations, combined with the extremely negative εHf in Paleoproterozoic and Paleozoic grains, suggest a source area in the northeastern Canadian Shield or Greenland rather than in Scandinavia or western Laurentia. Arctic terranes that contain early Paleozoic magmatic and sedimentary rocks with Precambrian detrital zircon U-Pb age spectra similar to those of the YAC, such as Pearya (Hadlari et al., 2014; Malone et al., 2014), the Canadian Arctic Islands (Anfinson et al., 2012), and Arctic Alaska (Miller et al., 2011), are not a likely source for the early Paleozoic detrital zircons in the YAC because these areas contain zircons in the age range of 700–500 Ma, which are not common in YAC rocks, and the $\varepsilon Hf_{(t)}$ values for Paleozoic zircons are dominantly positive (e.g., Franklinian field in Fig. 12) (Anfinson et al., 2012).

Our constraints on the age of deformation and metamorphism (ca. 410–400 Ma) require a position in the hanging wall of an early Paleozoic subduction system such as the Appalachian-Caledonide belt. The Early Devonian ages postdate the peak Caledonian collision and metamorphic events ca. 425 Ma (e.g., Roberts, 2003); however, evidence of later magmatism and metamorphism in northeast Greenland (Gilotti et al., 2004; Gilotti and McClelland, 2007) suggests that tectonism in this part of the orogen lasted to ca. 360 Ma. Deformation in the YAC is older than the Antler orogeny in southwestern Laurentia and the Ellesmerian orogeny in Arctic Laurentia (Fig. 13). The age of deformation in some Arctic terranes, e.g., the late Silurian to Early Devonian in Pearya (Trettin, 1991) and the Early Devonian Romanzof orogeny in Arctic Alaska (Lane, 2007) is similar to that within the YAC, although the U-Pb and Hf data seem to rule out specific correlations.

We thus interpret the YAC as an arc with associated arc-proximal detritus constructed on passive margin strata of northern or northeastern Laurentia, after the Caledonian collision and prior to or early in the development of the convergent margin arc in northwestern Laurentia (Fig. 13). Due to Mesozoic structural disruption of the YAC we cannot discern whether the arc developed on a rifted fragment of continental basement or in an Andean type setting, but the relatively coarse debris and negative $\varepsilon Hf_{(t)}$ in the arkosic paragneiss suggest proximity to exposed or reworked Mesoarchean to Eoarchean crust. In search of a source for early Paleozoic arcs with similar characteristics, we extend our comparison to other early Paleozoic arc terranes along the Cordilleran margin.

Comparisons to Peri-Laurentian and Exotic Early Paleozoic Arc Terranes

The geologic history of the YAC invites comparison to the Yukon-Tanana and Alexander terranes (Fig. 1; as discussed by, e.g., Gehrels et al., 1991; Brown et al., 2010). Brown et al. (2010) emphasized the passive margin character of the YAC paragneiss based on the quartzose-carbonate lithology and U-Pb data from one paragneiss sample (YA2) that contains abundant western Laurentian detritus and the youngest zircons, 1000 Ma (Brown and Gehrels, 2007). Brown et al. (2010) found age and lithologic similarities to paragneiss in the Yukon-Tanana terrane (Tracy Arm, Snowcap, and Dorsey assemblages; Colpron et al., 2006; Gehrels, 2001; Gehrels et al., 1991; Piercey and Colpron, 2009; Roots et al., 2006) and the Chase formation of the Okanagan region of British Columbia (Lemieux et al., 2007; Thompson et al., 2006). These inferred correlatives contain similar Precambrian age patterns but do not contain Paleozoic zircons as we have documented herein, raising the possibility that the YAC is correlative to younger rocks in the Yukon-Tanana terrane.

New data on the Yukon-Tanana terrane (Pecha et al., 2016) confirm that parts of this terrane have U-Pb and Hf characteristics similar to those of the YAC (Fig. 14). Although the age-Hf patterns of the Silurian–Devonian Endicott Arm assemblage are very similar to the combined YAC terrane data (Fig. 14), lithologically the Endicott Arm assemblage is dominated by mafic to felsic metavolcanic rocks, volcaniclastic metagraywacke, minor marble, and felsic to intermediate metaplutonic rocks (Pecha et al., 2016), in contrast to the predominantly quartzose carbonate strata of the YAC. The high $\varepsilon Hf_{(t)}$ in the broad peak of grains from 1.6 to 1.0 Ga, while similar between the terranes, is not a unique match, as several other terranes contain this signature. Separately comparing calc-silicate and arkose data to those of the Endicott Arm assemblage shows that the calc-silicate pattern is similar to the Endicott Arm assemblage, while the arkose pattern is more similar to the Tracy Arm Assemblage (Fig. 14). Differences between the YAC and Yukon-Tanana terranes are evident in the comparison of Paleozoic zircon data. Ordovician to Early Devonian zircons in the Yukon-Tanana terrane have much higher $\varepsilon Hf_{(t)}$ than those in the YAC (Fig. 14). The bulk of Yukon-Tanana terrane magmatism starts and ends later than in the YAC, but the younger magmatic rocks may overlap in age with the Devonian and younger parts of Chilliwack terrane that are not included in our study (Brown et al., 2010). It is possible that the YAC represents a basinal assemblage adjacent to the Endicott Arm assemblage arc, with the arkose representing erosion either from the Tracy Arm assemblage or the same provenance. Younger plutons of the Chilliwack terrane might represent migration of the arc into the former basin.

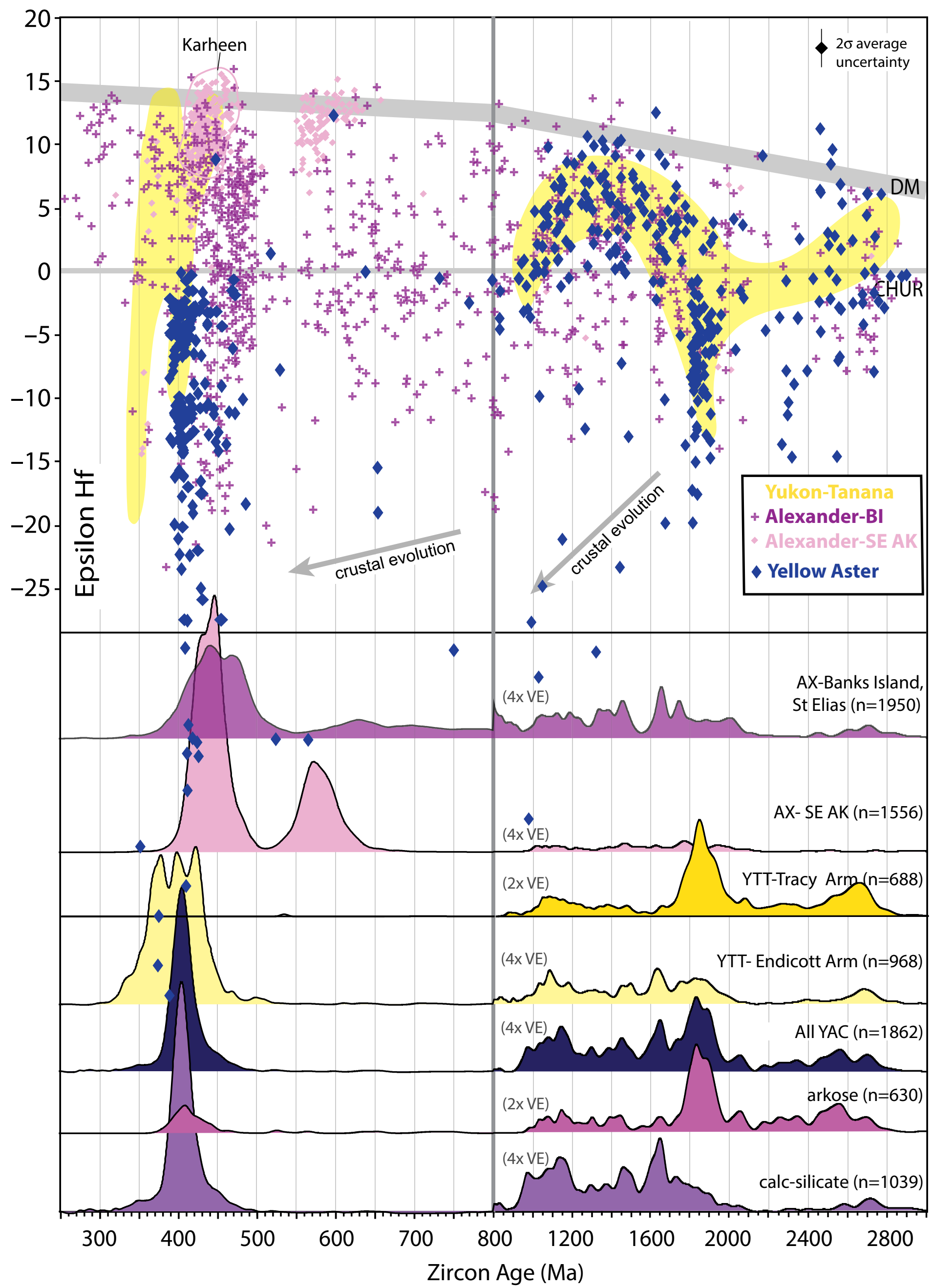

Figure 14. U-Pb and Hf comparison of the Yellow Aster Complex (YAC) with Yukon-Tanana (YTT) and Alexander terranes. DM—depleted mantle; CHUR—chondritic uniform reservoir; VE—vertical exaggeration. All YAC includes all samples reported in this study. Endicott Arm and Tracy Arm of Yukon-Tanana terrane data are from Pecha et al. (2016). Devonian and older sedimentary and volcanic rocks of Alexander terrane are shown in two colors: Alexander-BI shows Hf and U-Pb data from Banks Island and St. Elias Mountains (Tochilin et al., 2014; Beranek et al., 2012, 2013a, 2013b, respectively); Alexander SE AK—from southeastern Alaska portion of the terrane (White et al., 2016). Note change of X-axis scale at 800 Ma.

An alternative possibility, suggested by the age-Hf patterns in Figure 14, is that the YAC is a fragment of the Alexander terrane. The geological history of the Alexander terrane includes Neoproterozoic–early Paleozoic arc magmatism, and evidence for two early Paleozoic orogenic events, the Wales orogeny in late Cambrian to Ordovician time and the Klakas orogeny in Silurian time (e.g., Gehrels and Saleeby, 1987). Early Devonian clastic rocks (Karheen Formation) containing both cratonal debris and Paleozoic arc debris overlie the older deformed sequence. The Alexander terrane consists of a juvenile arc portion, predominantly in southeastern Alaska, and a coeval shelf facies exposed in the St. Elias Mountains (Beranek et al., 2013a, 2013b). Similar shelf facies rocks are exposed in southernmost Alexander terrane in the Banks Island assemblage (Tochilin et al., 2014). The Alexander terrane is now widely regarded to have had a Neoproterozoic to early Paleozoic history on the Arctic margin of Baltica based on faunal, lithologic, structural, paleomagnetic, age, and Hf isotope data, followed by westward translation to the Pacific margin and southward displacement along the Cordilleran margin (Soja, 1994; Bazard et al., 1995; Gehrels et al., 1996; Butler et al., 1997; Soja and Krutikov, 2008; Colpron and Nelson, 2009, 2011; Miller et al., 2011; Beranek et al., 2012, 2013b; Tochilin et al., 2014; White et al., 2016; Strauss et al., 2017). Pecha et al. (2016) inferred a possible connection between the southern Yukon-Tanana and Alexander terrane during early Paleozoic time based on similar age and Hf isotopes of Silurian magmatic rocks; they concluded that during early Paleozoic time, these two terranes were along the same subduction zone extending from Arctic Greenland (Alexander terrane) to northwest Laurentia (southern Yukon-Tanana) (Fig. 15).

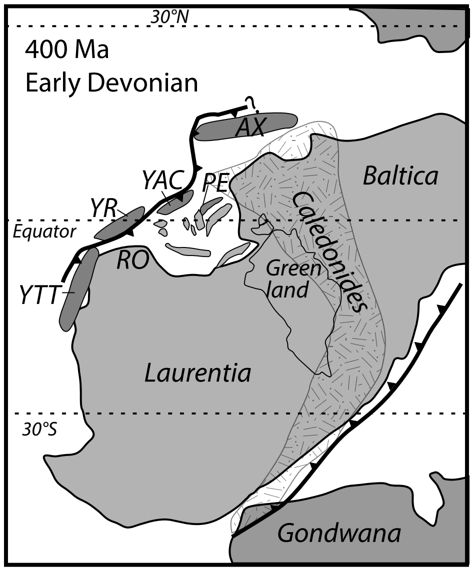

Figure 15. Early Devonian reconstruction showing possible locations for the Yellow Aster Complex (YAC) and related terranes. Inferred locations of Yukon-Tanana (YTT) and Alexander (AX) terranes are after Pecha et al. (2016). Continents, subduction zones, and Pearya (PE) terrane after Cocks and Torsvik (2011). Yreka (YR) and Romanzof orogen (RO) after Colpron and Nelson (2011).

YAC magmatism is largely younger than the Alexander terrane but older than the Yukon-Tanana terrane, and the YAC contains detrital and igneous inherited zircons of the Ordovician–Silurian arc. Similarities in lithology and age-Hf patterns exist between the YAC, the Icefield assemblage of the St. Elias Mountains (Beranek et al., 2013b), and the Banks Island assemblage (Tochilin et al., 2014). The Icefield assemblage is described as Cambrian to Middle Devonian sandstone, conglomerate, shale, sandy limestone, and minor lava flows and tuff deposited in a shallow marine to terrestrial environment (Beranek et al., 2013b). The Banks Island assemblage consists of quartzose metasedimentary rocks and marble of Ordovician–Devonian and Permian ages (Tochilin et al., 2014). Comparison of these two terranes with the YAC suggests strong similarity, in particular with strata of Silurian to Early Devonian age in the St. Elias Mountains (Beranek et al., 2013b), and somewhat less strong similarity with the quartzite-marble samples of Banks Island assemblage that have maximum depositional ages of 450–438 Ma (Tochilin et al., 2014). These particular samples do not contain the 700–500 Ma Timanide peak that is found in older (Cambrian to Ordovician) samples. Our earlier speculation that the YAC was equivalent to the Karheen Formation in the Alexander terrane based on nearly identical U-Pb age patterns and some lithological similarities (Hoffnagle, 2014; Hoffnagle et al., 2014) is now ruled out by the uniformly positive $\varepsilon Hf_{(t)}$ in Paleozoic zircons from the Karheen Formation (Tochilin et al., 2014), versus negative $\varepsilon Hf_{(t)}$ for zircons of the same age in the YAC (Fig. 14).

If the YAC is related to the St. Elias–Banks Island portion of the Alexander terrane, it would have originated along the Arctic margin of Laurentia and/or Baltica in pre–Early Devonian time (Beranek et al., 2013b; Tochilin et al., 2014), for which we have a sparse record [consisting only of sample YA2 of Brown and Gehrels (2007) and possibly two of the YAC paragneiss protoliths]. Early Devonian arc development along the Arctic margin would have shed arc debris, Caledonian metamorphic debris, and reworked Archean, Paleoproterozoic, and Mesoproterozoic grains onto the shelf where quartzose-carbonate strata had accumulated. Recent models for transporting the Alexander terrane through the northwest passage westward along Arctic Laurentia (Colpron and Nelson, 2009, 2011; Beranek et al., 2013b; White et al., 2016) place the Alexander terrane off western Laurentia by Late Devonian time, after which it became part of the fringing middle to late Paleozoic arc system outboard of the Slide Mountain ocean.

Whether the YAC is more closely related to the Yukon-Tanana or Alexander terranes, or was located along the early Paleozoic subduction zone somewhere between the Alexander and Yukon-Tanana terranes, it was likely displaced southward by sinistral faulting during the Mesozoic (Monger et al., 1994; Gehrels et al., 2009; Tochilin et al., 2014; Yokelson et al., 2015). Later (mid-Cretaceous) northward displacement is suggested by the model of Brown (1987, 2012) for margin-parallel shortening and emplacement of the Northwest Cascades thrust system, the thrust system that contains the YAC blocks.

The YAC has also been compared to early Paleozoic arc and sedimentary sequences that were accreted further south along the Cordilleran margin (Brown et al., 2010). Possible correlative assemblages in the Klamath and

Sierra Nevada Mountains include the Yreka subterrane (Eastern Klamath terrane) and the Shoofly assemblage in the Northern Sierra terrane, both of which were interpreted by Grove et al. (2008) to have originated as components of the exotic (non-Laurentian) early Paleozoic convergent margin displaced from Baltica, and possibly related to the Alexander terrane. We can compare these terranes against our new U-Pb results, but because no new Hf data have been published, any links remain tentative. Lithologically, the YAC most closely resembles the Early Devonian Moffet Creek Formation in the Yreka subterrane of the Eastern Klamath terrane, which consists of Early Devonian calcareous metasiltstone and sandstone that varies from quartz arenite to feldspathic wacke (Hotz, 1977). Precambrian age patterns for the calc-silicate unit of the YAC are similar to those of the Yreka subterrane, in particular to the Early Devonian Moffet Creek and Duzel Phyllite units (Grove et al., 2008). However, the Yreka terrane U-Pb patterns do not resemble that of the arkosic paragneiss of the YAC. Early Paleozoic volcanic arc detritus is abundant in Early Devonian strata of the Eastern Klamath and Northern Sierra terranes and, as in the YAC, some samples are dominated by Paleozoic zircons while others contain predominantly Precambrian zircons (Grove et al., 2008). Grove et al. (2008) concluded that Alexander, Eastern Klamath, and Northern Sierra terranes originated at the same convergent margin, although not necessarily from the same location or via the same transport history.

Detritus similar to the constituents of the YAC and other early Paleozoic arcs occurs in the westward-derived Late Devonian Sassenach formation of the southern British Columbia passive margin (Gehrels and Pecha, 2014), and unexplained Devonian deformation occurs in the Purcell Mountains of southern British Columbia (Root, 2001); both of these events could be related to the arrival of the YAC or similar terranes that are currently further south (Colpron and Nelson, 2009). Furthermore, clastic material shed from the Antler orogenic belt is of similar detrital zircon pattern to the exotic arcs, and sparse Hf data (Beranek et al., 2016) in the Antler overlap assemblage in Idaho suggest derivation from an early Paleozoic arc with strongly negative $\varepsilon Hf_{(t)}$. The arrival of early Paleozoic arc terranes off western Laurentia by Late Devonian time is supported by detrital zircons in Late Devonian and younger strata of the passive margin (Gehrels and Pecha, 2014).

CONCLUSIONS

Geologic, geochronologic, and Hf isotope data from the YAC provide a detailed history that can be compared with other early Paleozoic arc terranes of the western North American Cordillera. The oldest components of the terrane are paragneisses, the protoliths of which are calc-silicate rocks and arkosic sandstone and conglomerate containing significant Ordovician to Early Devonian zircon populations in addition to abundant Precambrian grains. Maximum depositional ages range from Ordovician to Early Devonian (432–390 Ma). Hf isotope data on early Paleozoic detrital zircons with $\varepsilon Hf_{(t)}$ values of –50 to –57 indicate that the source area was an arc developed on or near early Eoarchean crust. Paragneiss was intruded by pre-tectonic, syn-tectonic, and post-tectonic plutons dated as 411–395 Ma. Sedimentation, magmatism, metamorphism, and deformation broadly overlapped in time from ca. 415 to 390 Ma during the Early Devonian, suggesting that although the arc may have developed on earlier passive margin rocks, those older rocks are only sparsely (if at all) preserved in the YAC. Age and Hf isotope patterns suggest that the early Paleozoic YAC arc was part of an extensive convergent margin developed offshore of Greenland and northern Laurentia. Similarities and differences between the Yukon-Tanana and Alexander terranes suggest a possible setting on the continental side of the arc, similar to the Banks Island and St. Elias components of the Alexander terrane. If our inferences of origin are correct, the YAC must have been displaced westward along the Arctic margin and then southward along the Cordilleran margin during Paleozoic and Mesozoic time.

ACKNOWLEDGMENTS

We thank Peter Dykes, Matt Holland, Kenny Frank, Marley Kirkham, Brandon Brayfield, and Austin Hart for field and laboratory support. Funding was provided by the Geological Society of America and Western Washington University to Hoffnagle, National Science Foundation (NSF) grant EAR-133853 to the Arizona LaserChron Center, NSF grant EAR-1249115 to Schermer and Brown, and NSF grant EAR-1242939 to Gehrels. Reviews by Associate Editor G. Lang Farmer and two anonymous reviewers helped us improve the manuscript.

REFERENCES CITED

Andersen, T., 2013, Age, Hf isotope and trace element signatures of detrital zircons in the Mesoproterozoic Eriksfjord sandstone, southern Greenland: Are detrital zircons reliable guides to sedimentary provenance and timing of deposition?: Geological Magazine, v. 150, p. 426–440, https://doi.org/10.1017/S0016756812000623.

Andersen, T., Griffin, W.L., and Pearson, N.J., 2002, Crustal Evolution in the SW part of the Baltic Shield: The Hf isotope evidence: Journal of Petrology, v. 43, p. 1725–1747, https://doi.org/10.1093/petrology/43.9.1725.

Andersen, T., Griffin, W.L., and Sylvester, A.G., 2007, Sveconorwegian crustal underplating in southwestern Fennoscandia: LAM-ICPMS U-Pb and Lu-Hf isotope evidence from granites and gneisses in Telemark, southern Norway: Lithos, v. 93, p. 273–287, https://doi.org/10.1016/j.lithos.2006.03.068.

Andersen, T., Saeed, A., Gabrielsen, R.H., and Olaussen, S., 2011, Provenance characteristics of the Brumunddal sandstone in the Oslo Rift derived from U-Pb, Lu-Hf and trace element analyses of detrital zircons by laser ablation ICMPS: Norsk Geologisk Tidsskrift, v. 91, p. 1–19.

Andresen, A., Agyei-Dwarko, N.Y., Kristoffersen, M., and Hanken, N.-M., 2014, A Timanian foreland basin setting for the late Neoproterozoic–early Palaeozoic cover sequences (Dividal Group) of northeastern Baltica, *in* Corfu, F., et al., eds., New Perspectives on the Caledonides of Scandinavia and Related Areas: Geological Society of London Special Publication 390, p. 157–175, https://doi.org/10.1144/SP390.29.

Anfinson, O.A., Leier, A.L., Gaschnig, R., Embry, A.F., and Dewing, K., 2012, U-Pb and Hf isotopic data from Franklinian Basin strata; insights into the nature of Crockerland and the timing of accretion, Canadian Arctic Islands: Canadian Journal of Earth Sciences, v. 49, p. 1316–1328, https://doi.org/10.1139/e2012-067.

Appleby, S.K., Gillespie, M.R., Graham, C.M., Hinton, R.W., Oliver, G.J.H., and Kelly, N.M., 2010, Do S-type granites commonly sample infracrustal sources? New results from an integrated O, U-Pb and Hf isotope study of zircon: Contributions to Mineralogy and Petrology, v. 160, p. 115–132, https://doi.org/10.1007/s00410-009-0469-3.

Augland, L.E., Andresen, A., Corfu, F., and Daviknes, H.K., 2012a, Late Ordovician to Silurian ensialic magmatism in Liverpool Land, East Greenland: New evidence extending the northeastern branch of the continental Laurentian magmatic arc: Geological Magazine, v. 149, p. 561–577, https://doi.org/10.1017/S0016756811000781.

Augland, L.E., Andresen, A., Corfu, F., Simonsen, S.L., and Andersen, T., 2012b, The Beiarn Nappe Complex: A record of Laurentian Early Silurian arc magmatism in the Uppermost Allochthon, Scandinavian Caledonides: Lithos, v. 146–147, p. 233–252, https://doi.org/10.1016/j.lithos.2012.05.016.

Augland, L.E., Andresen, A., Corfu, F., Agyei-Dwarko, N.Y., and Larionov, A.N., 2014a, The Bratten-Landegode gneiss complex: A fragment of Laurentian continental crust in the Uppermost Allochthon of the Scandinavian Caledonides, *in* Corfu, F., et al., eds., New Perspectives on the Caledonides of Scandinavia and Related Areas: Geological Society of London Special Publication 390, p. 633–654, https://doi.org/10.1144/SP390.1.

Augland, L.E., Andresen, A., Gasser, D., and Steltenpohl, M.G., 2014b, Early Ordovician to Silurian evolution of exotic terranes in the Scandinavian Caledonides of the Ofoten-Troms area—Terrane characterization and correlation based on new U-Pb zircon ages and Lu-Hf isotopic data, *in* Corfu, F., et al., eds., New Perspectives on the Caledonides of Scandinavia and Related Areas: Geological Society of London Special Publication 390, p. 655–678, https://doi.org/10.1144/SP390.19.

Bazard, D.R., Butler, R.F., Gehrels, G., and Soja, C.M., 1995, Early Devonian paleomagnetic data from the Lower Devonian Karheen Formation suggest Laurentia-Baltica connection for the Alexander terrane: Geology, v. 23, p. 707–710, https://doi.org/10.1130/0091-7613(1995)023<0707:EDPDFT>2.3.CO;2.

Beranek, L.P., van Staal, C.R., Gordee, S.M., McClelland, W.C., Israel, S., and Mihalynuk, M., 2012, Tectonic significance of Upper Cambrian–Middle Ordovician mafic volcanic rocks on the Alexander terrane, Saint Elias Mountains, northwestern Canada: Journal of Geology, v. 120, p. 293–314, https://doi.org/10.1086/664788.

Beranek, L.P., van Staal, C.R., McClelland, W.C., Israel, S., and Mihalynuk, M.G., 2013a, Baltican crustal provenance for Cambrian–Ordovician sandstones of the Alexander terrane, North American Cordillera: Evidence from detrital zircon U-Pb geochronology and Hf isotope geochemistry: Journal of the Geological Society [London], v. 170, p. 7–18, https://doi.org/10.1144/jgs2012-028.

Beranek, L.P., van Staal, C.R., McClelland, W.C., Israel, S., and Mihalynuk, M.G., 2013b, Detrital zircon Hf isotopic compositions indicate a northern Caledonian connection for the Alexander terrane: Lithosphere, v. 5, p. 163–168, https://doi.org/10.1130/L255.1.

Beranek, L.P., Link, P.K., and Fanning, C.M., 2016, Detrital zircon record of mid-Paleozoic convergent margin activity in the northern U.S. Rocky Mountains: Implications for the Antler orogeny and early evolution of the North American Cordillera: Lithosphere, v. 8, p. 533–550, https://doi.org/10.1130/L557.1.

Bingen, B., and Solli, A., 2009, Geochronology of magmatism in the Caledonian and Sveconorwegian belts of Baltica: synopsis for detrital zircon provenance studies: Norsk Geologisk Tidsskrift, v. 89, p. 267–290.

Blackwell, D.L., 1983, Geology of the Park Butte–Loomis Mountain area, Washington (eastern margin of the Twin Sisters dunite) [M.S. thesis]: Bellingham, Western Washington University, 253 p.

Bouvier, A., Vervoort, J.D., and Patchett, P.J., 2008, The Lu-Hf and Sm-Nd isotopic composition of CHUR: Constraints from unequilibrated chondrites and implications for the bulk composition of terrestrial planets: Earth and Planetary Science Letters, v. 273, p. 48–57, https://doi.org/10.1016/j.epsl.2008.06.010.

Brander, L., Söderlund, U., and Bingen, B., 2011, Tracing the 1271–1246 Ma Central Scandinavian Dolerite Group mafic magmatism in Fennoscandia: U-Pb baddeleyite and Hf isotope data on the Moslätt and Børgefjell dolerites: Geological Magazine, v. 148, p. 632–643, https://doi.org/10.1017/S0016756811000033.

Brandon, M.T., Cowan, D.S., and Vance, J.A., 1988, The Late Cretaceous San Juan Thrust System, San Juan Islands, Washington: Geological Society of America Special Paper 221, p. 83 p., https://doi.org/10.1130/SPE221.

Brown, E.H., 1987, Structural geology and accretionary history of the northwest Cascades system, Washington and British Columbia: Geological Society of America Bulletin, v. 99, p. 201–214, https://doi.org/10.1130/0016-7606(1987)99<201:SGAAHO>2.0.CO;2.

Brown, E.H., 2012, Obducted nappe sequence in the San Juan Islands–northwest Cascades thrust system, Washington and British Columbia: Canadian Journal of Earth Sciences, v. 49, p. 796–817, https://doi.org/10.1139/e2012-026.

Brown, E.H., and Dragovich, J.D., 2003, Tectonic elements and evolution of northwest Washington: Washington Division of Geology and Earth Resources Geologic Map GM-52, scale 1:625,000.

Brown, E.H., and Gehrels, G.E., 2007, Detrital zircon constraints on terrane ages and affinities and timing of orogenic events in the San Juan Islands and North Cascades, Washington: Canadian Journal of Earth Sciences, v. 44, p. 1375–1396, https://doi.org/10.1139/e07-040.

Brown, E.H., and Vance, J.A., 1987, Correlation of pre-Tertiary thrust structures between the San Juan Islands and northwest Cascades, Washington: Geological Society of America Abstracts with Programs, v. 19, p. 362.

Brown, E.H., Bernardi, M.L., Christenson, B.W., Cruver, J.R., Haugerud, R.H., Rady, P.M., and Sondergaard, J.N., 1981, Metamorphic facies and tectonics in part of the Cascade Range and Puget Lowland, northwestern Washington: Geological Society of America Bulletin, v. 92, p. 170–178, https://doi.org/10.1130/0016-7606(1981)92<170:MFATIP>2.0.CO;2.

Brown, E.H., Gehrels, G.E., and Valencia, V.A., 2010, Chilliwack composite terrane in northwest Washington: Neoproterozoic–Silurian passive margin basement, Ordovician–Silurian arc inception: Canadian Journal of Earth Sciences, v. 47, p. 1347–1366, https://doi.org/10.1139/E10-047.

Butler, R.F., Gehrels, G.E., and Bazard, D.R., 1997, Paleomagnetism of Paleozoic strata of the Alexander terrane, southeastern Alaska: Geological Society of America Bulletin, v. 109, p. 1372–1388, https://doi.org/10.1130/0016-7606(1997)109<1372:POPSOT>2.3.CO;2.

Cocks, L.R.M., and Torsvik, T.H., 2011, The Palaeozoic geography of Laurentia and western Laurussia: A stable craton with mobile margins: Earth-Science Reviews, v. 106, p. 1–51, https://doi.org/10.1016/j.earscirev.2011.01.007.

Colpron, M., and Nelson, J.L., 2009, A Palaeozoic Northwest Passage: Incursion of Caledonian, Baltican and Siberian terranes into eastern Panthalassa, and the early evolution of the North American Cordillera, *in* Cawood, P.A., and Kröner, A., eds., Earth Accretionary Systems in Space and Time: Geological Society of London Special Publication 318, p. 273–307, https://doi.org/10.1144/SP318.10.

Colpron, M., and Nelson, J.L., 2011, A Palaeozoic NW Passage and the Timanian, Caledonian and Uralian connections of some exotic terranes in the North American Cordillera, *in* Spencer, A.M., et al., eds., Arctic Petroleum Geology: Geological Society of London Memoir 35, p. 463–484, https://doi.org/10.1144/M35.31.

Colpron, M., Mortensen, J.K., Gehrels, G.E., and Villeneuve, M., 2006, Basement complex, Carboniferous magmatism and Paleozoic deformation in Yukon-Tanana terrane of central Yukon: Field, geochemical and geochronologic constraints from Glenlyon map area, *in* Colpron, N., and Nelson, J.L., eds., Paleozoic Evolution and Metallogeny of Pericratonic Terranes at the Ancient Pacific Margin of North America, Canadian and Alaskan Cordillera: Geological Association of Canada Special Paper 45, p. 131–151.

Corfu, F., and Hartz, E.H., 2011, U-Pb geochronology in Liverpool Land and Canning Land, East Greenland—The complex record of a polyphase Caledonian orogeny: Canadian Journal of Earth Sciences, v. 48, p. 473–494, https://doi.org/10.1139/E10-066.

Corfu, F., Gerber, M., Andersen, T.B., Torsvik, T.H., and Ashwal, L.D., 2011, Age and significance of Grenvillian and Silurian orogenic events in the Finnmarkian Caledonides, northern Norway: Canadian Journal of Earth Sciences, v. 48, p. 419–440, https://doi.org/10.1139/E10-043.

Cowan, D.S., and Brandon, M.T., 1994, A symmetry-based method for kinematic analysis of large-slip brittle fault zones: American Journal of Science, v. 294, p. 257–306, https://doi.org/10.2475/ajs.294.3.257.

Crawford, M.L., Hollister, L.S., and Woodsworth, G.J., 1987, Crustal deformation and regional metamorphism across a terrane boundary, Coast plutonic complex, British Columbia: Tectonics, v. 6, p. 343–361, https://doi.org/10.1029/TC006i003p00343.

Dickinson, W.R., and Gehrels, G.E., 2009, Use of U-Pb ages of detrital zircons to infer maximum depositional ages of strata: A test against a Colorado Plateau Mesozoic database: Earth and Planetary Science Letters, v. 288, p. 115–125, https://doi.org/10.1016/j.epsl.2009.09.013.

Flowerdew, M.J., Chew, D.M., Daly, J.S., and Millar, I.L., 2009, Hidden Archaean and Palaeoproterozoic crust in NW Ireland? Evidence from zircon Hf isotopic data from granitoid intrusions: Geological Magazine, v. 146, p. 903–916, https://doi.org/10.1017/S0016756809990227.

Gee, D.G., Ladenberger, A., Dahlqvist, P., Majka, J., Be'eri-Shlevin, Y., Frei, D., and Thomsen, T., 2014, The Baltoscandian margin detrital zircon signatures of the central Scandes, *in* Corfu, F., et al., eds., New Perspectives on the Caledonides of Scandinavia and Related Areas: Geological Society of London Special Publication 390, p. 131–155, https://doi.org/10.1144/SP390.20.

Gehrels, G.E., 2001, Geology of the Chatham Sound region, southeast Alaska and coastal British Columbia: Canadian Journal of Earth Sciences, v. 38, p. 1579–1599, https://doi.org/10.1139/e01-040.

Gehrels, G., and Pecha, M., 2014, Detrital zircon U-Pb geochronology and Hf isotope geochemistry of Paleozoic and Triassic passive margin strata of western North America: Geosphere, v. 10, p. 49–65, https://doi.org/10.1130/GES00889.1.

Gehrels, G.E., and Ross, G.M., 1998, Detrital zircon geochronology of Neoproterozoic to Permian miogeoclinal strata in British Columbia: Canadian Journal of Earth Sciences, v. 35, p. 1380–1401, https://doi.org/10.1139/e98-071.

Gehrels, G.E., and Saleeby, J.B., 1987, Geologic framework, tectonic evolution, and displacement history of the Alexander terrane: Tectonics, v. 6, p. 151–173, https://doi.org/10.1029/TC006i002p00151.

Gehrels, G.E., McClelland, W.C., Samson, S.D., and Patchett, P.J., 1991, U-Pb geochronology of detrital zircons from a continental margin assemblage in the northern Coast Mountains, southeastern Alaska: Canadian Journal of Earth Sciences, v. 28, p. 1285–1300, https://doi.org/10.1139/e91-114.

Gehrels, G.E., Dickinson, W.R., Ross, G.M., Stewart, J.H., and Howell, D.G., 1995, Detrital zircon reference for Cambrian to Triassic miogeoclinal strata of western North America: Geology, v. 23, p. 831–834, https://doi.org/10.1130/0091-7613(1995)023<0831:DZRFCT>2.3.CO;2.

Gehrels, G.E., Butler, R.F., and Bazard, D.R., 1996, Detrital zircon geochronology of the Alexander terrane, southeastern Alaska: Geological Society of America Bulletin, v. 108, p. 722–734, https://doi.org/10.1130/0016-7606(1996)108<0722:DZGOTA>2.3.CO;2.

Gehrels, G.E., Dickinson, W.R., Riley, B.C., Finney, S.C., and Smith, M.T., 2000, Detrital zircon geochronology of the Roberts Mountains allochthon, Nevada, *in* Soreghan, M.J., and Gehrels, G.E., eds., Paleozoic and Triassic Paleogeography and Tectonics of Western Nevada and Northern California: Geological Society of America Special Paper 347, p. 19–42, https://doi.org/10.1130/0-8137-2347-7.19.

Gehrels, G.E., Valencia, V., and Pullen, A., 2006, Detrital zircon geochronology by laser-ablation multicollector ICPMS at the Arizona LaserChron Center, *in* Loszewski, T., and Huff, W., eds., Geochronology: Emerging Opportunities: Paleontology Society Short Course: Paleontology Society Papers, v. 11, p. 10.

Gehrels, G.E., Valencia, V.A., and Ruiz, J., 2008, Enhanced precision, accuracy, efficiency, and spatial resolution of U-Pb ages by laser ablation-multicollector-inductively coupled plasma-mass spectrometry: Geochemistry, Geophysics, Geosystems, v. 9, https://doi.org/10.1029/2007GC001805.

Gehrels, G., et al., 2009, U-Th-Pb geochronology of the Coast Mountains batholith in north-coastal British Columbia: Constraints on age and tectonic evolution: Geological Society of America Bulletin, v. 121, p. 1341–1361, https://doi.org/10.1130/B26404.1.

Gilotti, J.A., and McClelland, W.C., 2007, Characteristics of, and a tectonic model for ultra-high-pressure metamorphism in the overriding plate of the Caledonian orogen: International Geology Review, v. 49, p. 777–797, https://doi.org/10.2747/0020-6814.49.9.777.

Gilotti, J.A., Nutman, A.P., and Brueckner, H.K., 2004, Devonian to Carboniferous collision in the Greenland Caledonides: U-Pb zircon and Sm-Nd ages of high-pressure and ultrahigh-pressure metamorphism: Contributions to Mineralogy and Petrology, v. 148, p. 216–235, https://doi.org/10.1007/s00410-004-0600-4.

Grove, M., Gehrels, G.E., Cotkin, S.J., Wright, J.E., and Zou, H., 2008, Non-Laurentian cratonal provenance of Late Ordovician eastern Klamath blueschists and a link to the Alexander terrane, *in* Wright, J.E., and Shervais, J.W., eds., Ophiolites, Arcs, and Batholiths: A Tribute to Cliff Hopson: Geological Society of America Special Paper 438, p. 223–250, https://doi.org/10.1130/2008.2438(08).

Hadlari, T., Davis, W.J., Dewing, K., Heaman, L.M., Lemieux, Y., Ootes, L., Pratt, B.R., and Pyle, L.J., 2012, Two detrital zircon signatures for the Cambrian passive margin of northern Laurentia highlighted by new U-Pb results from northern Canada: Geological Society of America Bulletin, v. 124, p. 1155–1168, https://doi.org/10.1130/B30530.1.

Hadlari, T., Davis, W.J., and Dewing, K., 2014, A pericratonic model for the Pearya terrane as an extension of the Franklinian margin of Laurentia, Canadian Arctic: Geological Society of America Bulletin, v. 126, p. 182–200, https://doi.org/10.1130/B30843.1.

Hadlari, T., Swindles, G.T., Galloway, J.M., Bell, K.M., Sulphur, K.C., Heaman, L.M., Beranek, L.P., and Fallas, K.M., 2015, 1.8 billion years of detrital zircon recycling calibrates a refractory part of Earth's sedimentary cycle: PLoS One, v. 10, e0144727, https://doi.org/10.1371/journal.pone.0144727.

Harms, T.A., Dewey, J.F., and Mange, M.A., 2003, A model for the Appalachian origin of Paleozoic terranes in the North American Cordillera: Geological Society of America Abstracts with Programs, v. 35, no. 6, p. 113.

Hoffnagle, E.A., 2014, Age, origin, and tectonic evolution of the Yellow Aster Complex: Northwest Washington state [M.S. thesis]: Bellingham, Western Washington University, 141 p., http://cedar.wwu.edu/wwuet/356/ (accessed October 2016).

Hoffnagle, E.A., Schermer, E.R., and Brown, E.H., 2014, Baltic, western Laurentian, and Early Devonian arc detritus in the Yellow Aster Complex of northwest Washington State: Geological Society of America Abstracts with Programs, v. 46, no. 6, p. 362.

Hotz, P.E., 1977, Geology of the Yreka Quadrangle, Siskiyou County California: U.S. Geological Survey Bulletin 1436, 72 p.

Kalsbeek, F., Higgins, A.K., Jepsen, H.F., Frei, R., and Nutman, A.P., 2008, Granites and granites in the East Greenland Caledonides, *in* Higgins, A.K., et al., eds., The Greenland Caledonides: Geological Society of America Memoir 202, p. 227–249, https://doi.org/10.1130/2008.1202(09).

Kirkham, M., 2015, Geochemical Analysis of Igneous units in the Yellow Aster Complex [B.S. thesis]: Bellingham, Western Washington University, 36 p.

Kristoffersen, M., Andersen, T., and Andresen, A., 2014, U-Pb age and Lu-Hf signatures of detrital zircon from Palaeozoic sandstones in the Oslo Rift, Norway: Geological Magazine, v. 151, p. 816–829, https://doi.org/10.1017/S0016756813000885.

Lane, L.S., 2007, Devonian–Carboniferous paleogeography and orogenesis, northern Yukon and adjacent Arctic Alaska: Canadian Journal of Earth Sciences, v. 44, p. 679–694, https://doi.org/10.1139/e06-131.

Lemieux, Y., Thompson, R.I., Erdmer, P., Simonetti, A., and Creaser, R.A., 2007, Detrital zircon geochronology and provenance of Late Proterozoic and mid-Paleozoic successions outboard of the miogeocline, southeastern Canadian Cordillera: Canadian Journal of Earth Sciences, v. 44, p. 1675–1693, https://doi.org/10.1139/e07-048.

Ludwig, K.R., 2008, User's Manual for Isoplot 3.6: A Geochronological Toolkit for Microsoft Excel: Berkeley Geochronology Center Special Publication 4.

Lundmark, A.M., Bue, E.P., Gabrielsen, R.H., Flaat, K., Strand, T., and Ohm, S.E., 2014, Provenance of late Palaeozoic terrestrial sediments on the northern flank of the Mid North Sea High: Detrital zircon geochronology and rutile geochemical constraints, *in* Scott, R.A., et al., eds., Sediment Provenance Studies in Hydrocarbon Exploration and Production: Geological Society of London Special Publication 386, p. 243–259, https://doi.org/10.1144/SP386.4.

Malone, S.J., McClelland, W.C., von Gosen, W., and Piepjohn, K., 2014, Proterozoic evolution of the North Atlantic–Arctic Caledonides: Insights from detrital zircon analysis of metasedimentary rocks from the Pearya Terrane, Canadian High Arctic: Journal of Geology, v. 122, p. 623–647, https://doi.org/10.1086/677902.

Mattinson, J.M., 1972, Ages of zircons from the northern Cascade Mountains, Washington: Geological Society of America Bulletin, v. 83, p. 3769–3784, https://doi.org/10.1130/0016-7606(1972)83[3769:AOZFTN]2.0.CO;2.

McClelland, W.C., Gehrels, G.E., and Saleeby, J.B., 1992, Upper Jurassic–Lower Cretaceous basinal strata along the Cordilleran margin: Implications for the accretionary history of the Alexander-Wrangellia-Peninsular terrane: Tectonics, v. 11, p. 823–835, https://doi.org/10.1029/92TC00241.

McGroder, M.F., 1991, Reconciliation of two-sided thrusting, burial metamorphism, and diachronous uplift in the Cascades of Washington and British Columbia: Geological Society of America Bulletin, v. 103, p. 189–209, https://doi.org/10.1130/0016-7606(1991)103<0189:ROTSTB>2.3.CO;2.

Miller, E.L., Kuznetsov, N., Soboleva, A., Udoratina, O., Grove, M.J., and Gehrels, G., 2011, Baltica in the Cordillera?: Geology, v. 39, p. 791–794, https://doi.org/10.1130/G31910.1.

Miller, M.M., 1987, Dispersed remnants of a northeast Pacific fringing arc: Upper Paleozoic terranes of Permian McCloud faunal affinity, western U.S.: Tectonics, v. 6, p. 807–830, https://doi.org/10.1029/TC006i006p00807.

Misch, P., 1966, Tectonic evolution of the northern Cascades of Washington State: A west-Cordilleran case history: Canadian Institute of Mining and Metallurgy Special Volume 8, p. 101–148.

Monger, J.W.H., van der Heyden, P., Journeay, J.M., Evenchick, C.A., and Mahoney, J.B., 1994, Jurassic–Cretaceous basins along the Canadian Coast belt: Their bearing on pre-mid-Cretaceous sinistral displacements: Geology, v. 22, p. 175–178, https://doi.org/10.1130/0091-7613(1994)022<0175:JCBATC>2.3.CO;2.

Mortensen, J.K., 1992, Pre-mid-Mesozoic tectonic evolution of the Yukon-Tanana terrane, Yukon and Alaska: Tectonics, v. 11, p. 836–853, https://doi.org/10.1029/91TC01169.

Nelson, J.L., Colpron, M., Piercy, S.J., Dusel-Bacon, C., Murphy, D.C., and Roots, C., 2006, Paleozoic tectonic and metallogenic evolution of pericratonic terranes in Yukon, northern British Columbia and eastern Alaska, *in* Colpron, M., and Nelson, J.L., eds., Paleozoic Evolution and Metallogeny of Pericratonic Terranes at the Ancient Pacific Margin of North America, Canadian and Alaskan Cordillera: Geological Association of Canada Special Paper 45, p. 323–360.

Patchett, P.J., 1983, Importance of the Lu-Hf isotopic system in studies of planetary chronology and chemical evolution: Geochimica et Cosmochimica Acta, v. 47, p. 81–91, https://doi.org/10.1016/0016-7037(83)90092-3.

Pecha, M.E., Gehrels, G.E., McClelland, W.C., Giesler, D., White, C., and Yokelson, I., 2016, Detrital zircon U-Pb geochronology and Hf isotope geochemistry of the Yukon-Tanana terrane, Coast Mountains, southeast Alaska: Geosphere, v. 12, p. 1556–1574, https://doi.org/10.1130/GES01303.1.

Piercey, S.J., and Colpron, M., 2009, Composition and provenance of the Snowcap assemblage, basement to the Yukon-Tanana terrane, northern Cordillera: Implications for Cordilleran crustal growth: Geosphere, v. 5, p. 439–464, https://doi.org/10.1130/GES00505.S3.

Rainbird, R.H., Hearnan, L.M., and Young, G., 1992, Sampling Laurentia: Detrital zircon geochronology offers evidence for an extensive Neoproterozoic river system originating from the Grenville orogen: Geology, v. 20, p. 351–354, https://doi.org/10.1130/0091-7613(1992)020<0351:SLDZGO>2.3.CO;2.

Rainbird, R., Cawood, P., and Gehrels, G., 2012, The great Grenvillian sedimentation episode: Record of supercontinent Rodinia's assembly, *in* Busby, C., and Azor, A., eds., Tectonics of Sedimentary Basins: Recent Advances: Chichester, UK, John Wiley & Sons, Ltd, p. 583–601, https://doi.org/10.1002/9781444347166.ch29.

Rasbury, E.T., and Walker, N.W., 1992, Implications of Sm-Nd model ages and single grain U-Pb zircon geochronology for the age and heritage of the Swakane Gneiss, Yellow Aster Complex, and Skagit Gneiss, North Cascades, Wash: Geological Society of America Abstracts with Programs, v. 24, no. 7, p. A65.

Rehnström, E.F., 2010, Prolonged Paleozoic Magmatism in the East Greenland Caledonides: Some Constraints from U-Pb Ages and Hf Isotopes: Journal of Geology, v. 118, p. 447–465, https://doi.org/10.1086/655010.

Roberts, D., 2003, The Scandinavian Caledonides: Event chronology, palaeogeographic settings and likely modern analogues: Tectonophysics, v. 365, p. 283–299, https://doi.org/10.1016/S0040-1951(03)00026-X.

Roberts, R.J., Corfu, F., Torsvik, T.H., Hetherington, C.J., and Ashwal, L.D., 2010, Age of alkaline rocks in the Seiland Igneous Province, northern Norway: Journal of the Geological Society [London], v. 167, p. 71–81, https://doi.org/10.1144/0016-76492009-014.

Røhr, T.S., Andersen, T., and Dypvik, H., 2008, Provenance of Lower Cretaceous sediments in the Wandel Sea Basin, north Greenland: Journal of the Geological Society [London], v. 165, p. 755–767, https://doi.org/10.1144/0016-76492007-102.

Root, K.G., 2001, Devonian Antler fold and thrust belt and foreland basin development in the southern Canadian Cordillera: implications for the Western Canada Sedimentary Basin: Bulletin of Canadian Petroleum Geology, v. 49, p. 7–36, https://doi.org/10.2113/49.1.7.

Roots, C., Nelson, J.L., Simard, R., and Harms, T.A., 2006, Continental fragments, mid-Paleozoic arcs and overlapping late Paleozoic arc and Triassic sedimentation in the Yukon-Tanana terrane of northern British Columbia and southern Yukon, *in* Colpron, M., and Nelson, J.L., eds., Paleozoic Evolution and Metallogeny of Pericratonic Terranes at the Ancient Pacific Margin of North America, Canadian and Alaskan Cordillera: Geological Association of Canada Special Paper 45, p. 153–177.

Ross, G.M., and Villeneuve, M., 2003, Provenance of Mesoproterozoic (1.45 Ga) Belt basin (western North America): Another piece in the pre-Rodinia paleogeographic puzzle: Geological Society of America Bulletin, v. 115, p. 1191–1217, https://doi.org/10.1130/B25209.1.

Rubin, C.M., and Saleeby, J.B., 1992, Tectonic history of the eastern edge of the Alexander terrane, southeast Alaska: Tectonics, v. 11, p. 586–602, https://doi.org/10.1029/91TC02182.

Rubin, C.M., Miller, M.M., and Smith, G.M., 1990a, Tectonic development of Cordilleran mid-Paleozoic volcano-plutonic complexes; evidence for convergent margin tectonism, *in* Harwood, D.S., and Miller, M.M., eds., Paleozoic and Early Mesozoic Paleogeographic Relations; Sierra Nevada, Klamath Mountains, and Related Terranes: Geological Society of America Special Paper 255, p. 1–16, https://doi.org/10.1130/SPE255-p1.

Rubin, C.M., Saleeby, J.B., Cowan, D.S., Brandon, M.T., and McGroder, M.F., 1990b, Regionally extensive mid-Cretaceous west-vergent thrust system in the northwestern Cordillera: Implications for continent-margin tectonism: Geology, v. 18, p. 276–280, https://doi.org/10.1130/0091-7613(1990)018<0276:REMCWV>2.3.CO;2.

Scherer, E., Münker, C., and Mezger, K., 2001, Calibration of the lutetium-hafnium clock: Science, v. 293, p. 683–687, https://doi.org/10.1126/science.1061372.

Sevigny, J.H., 1983, Structure and petrology of the Tomyhoi Peak area, North Cascade Range, Washington [M.S. thesis]: Bellingham, Western Washington University, 203 p.

Slama, J., and Pedersen, R.B., 2015, Zircon provenance of SW Caledonian phyllites reveals a distant Timanian sediment source: Journal of the Geological Society [London], v. 172, p. 465–478, https://doi.org/10.1144/jgs2014-143.

Slama, J., Walderhaug, O., Fonneland, H., Kosler, J., and Pedersen, R.B., 2011, Provenance of Neoproterozoic to upper Cretaceous sedimentary rocks, eastern Greenland: Implications for recognizing the sources of sediments in the Norwegian Sea: Sedimentary Geology, v. 238, p. 254–267, https://doi.org/10.1016/j.sedgeo.2011.04.018.

Söderlund, U., Patchett, P.J., Vervoort, J.D., and Isachsen, C.E., 2004, The ^{176}Lu decay constant determined by LU-Hf and U-Pb isotope systematics of Precambrian mafic intrusions: Earth and Planetary Science Letters, v. 219, p. 311–324, https://doi.org/10.1016/S0012-821X(04)00012-3.

Soja, C.M., 1994, Significance of Silurian stromatolite-sphinctozoan reefs: Geology, v. 22, p. 355–358, https://doi.org/10.1130/0091-7613(1994)022<0355:SOSSSR>2.3.CO;2.

Soja, C.M., 2008, Silurian-bearing terranes of Alaska, *in* Blodgett, R.B., and Stanley, G.D., eds., The Terrane Puzzle: New Perspectives on Paleontology and Stratigraphy from the North American Cordillera: Geological Society of America Special Paper 442, p. 39–50, https://doi.org/10.1130/2008.442(02).

Soja, C.M., and Antoshkina, A.I., 1997, Coeval development of Silurian stromatolite reefs in Alaska and the Ural Mountains: Implications for paleogeography of the Alexander terrane: Geology, v. 25, p. 539–542, https://doi.org/10.1130/0091-7613(1997)025<0539:CDOSSR>2.3.CO;2.

Soja, C.M., and Krutikov, L., 2008, Provenance, depositional setting, and tectonic implications of Silurian polymictic conglomerates in Alaska's Alexander terrane, *in* Blodgett, R.B., and Stanley, G.D., eds., The Terrane Puzzle: New Perspectives on Paleontology and Stratigraphy from the North American Cordillera: Geological Society of America Special Paper 442, p. 63–75, https://doi.org/10.1130/2008.442(04).

Stacey, J.S., and Kramers, J.D., 1975, Approximation of terrestrial lead isotope evolution by a two-stage model: Earth and Planetary Science Letters, v. 26, p. 207–221, https://doi.org/10.1016/0012-821X(75)90088-6.

Stevenson, R.K., and Patchett, P.J., 1990, Implications for the evolution of continental crust from Hf isotope systematics of Archean detrital zircons: Geochimica et Cosmochimica Acta, v. 54, p. 1683–1697, https://doi.org/10.1016/0016-7037(90)90400-F.

Stevenson, R.K., Whittaker, S., and Mountjoy, E.W., 2000, Geochemical and Nd isotopic evidence for sedimentary source changes in the Devonian miogeocline of the southern Canadian Cordillera: Geological Society of America Bulletin, v. 112, p. 531–539, https://doi.org/10.1130/0016-7606(2000)112<531:GANIEF>2.0.CO;2.

Strauss, J.V., Hoiland, C.W., Ward, W.P., Johnson, B.G., Nelson, L.L., and McClelland, W.C., 2017, Orogen transplant: Taconic–Caledonian arc magmatism in the central Brooks Range of Alaska: Geological Society of America Bulletin, v. 129, p. 649–676, https://doi.org/10.1130/B31593.1.

Tabor, R.W., Haugerud, R.A., Hildreth, W., and Brown, E.H., 2003, Geologic Map of the Mt Baker 30- by 60 Minute Quadrangle, Washington: U.S. Geological Survey Miscellaneous Investigations Map I-2660, scale 1:100,000.

Thompson, R.I., Glombick, P., Erdmer, P., Heaman, L.M., Lemieux, Y., and Daughtry, K.L., 2006, Evolution of the ancestral Pacific margin, southern Canadian Cordillera: Insights from new geologic maps, *in* Colpron, M., and Nelson, J.L., eds., Paleozoic Evolution and Metallogeny of Pericratonic Terranes at the Ancient Pacific Margin of North America, Canadian and Alaskan Cordillera: Geological Association of Canada Special Paper 45, p. 433–482.

Tochilin, C.J., Gehrels, G.E., Nelson, J., and Mahoney, J.B., 2014, U-Pb and Hf isotope analysis of detrital zircons from the Banks Island assemblage (coastal British Columbia) and southern Alexander terrane (southeast Alaska): Lithosphere, v. 6, p. 200–215, https://doi.org/10.1130/L338.1.

Trettin, H.P., 1991, Late Silurian–Early Carboniferous deformational phases and associated metamorphism and plutonism, Arctic Islands, *in* Trettin, H.P., ed., Geology of the Innuitian Orogen and Arctic Platform of Canada and Greenland, Ottawa: Geological Survey of Canada, Geology of Canada, v. 3, p. 337–341.

van der Heyden, P., 1992, A Middle Jurassic to early Tertiary Andean-Sierran subduction model for the Coast Belt of British Columbia: Tectonics, v. 11, p. 82–97, https://doi.org/10.1029/91TC02183.

Van Schmus, W.R., et al., 1993, Transcontinental Proterozoic provinces, *in* Reed, J.C., Jr., et al., eds., Precambrian: Conterminous U.S.: Boulder, Colorado, Geological Society of America, Geology of North America, v. C-2, p. 171–334, https://doi.org/10.1130/DNAG-GNA-C2.171.
Vervoort, J.D., and Blichert-Toft, J., 1999, Evolution of the depleted mantle: Hf isotope evidence from juvenile rocks through time: Geochimica et Cosmochimica Acta, v. 63, p. 533–556, https://doi.org/10.1016/S0016-7037(98)00274-9.
Vervoort, J.D., and Patchett, P.J., 1996, Behavior of hafnium and neodymium isotopes in the crust: Constraints from Precambrian crustally derived granites: Geochimica et Cosmochimica Acta, v. 60, p. 3717–3733, https://doi.org/10.1016/0016-7037(96)00201-3.
Vervoort, J.D., Patchett, P.J., Blichert-Toft, J., and Albarède, F., 1999, Relationships between Lu-Hf and Sm-Nd isotopic systems in the global sedimentary system: Earth and Planetary Science Letters, v. 168, p. 79–99, https://doi.org/10.1016/S0012-821X(99)00047-3.
Vervoort, J.D., Patchett, P.J., Söderlund, U., and Baker, M., 2004, Isotopic composition of Yb and the determination of Lu concentrations and Lu/Hf ratios by isotope dilution using MC-ICPMS: Geochemistry, Geophysics, Geosystems, v. 5, Q11002, https://doi.org/10.1029/2004GC000721.
Whetten, J.T., Jones, D.L., Cowan, D.S., and Zartman, R.E., 1978, Ages of Mesozoic terranes in the San Juan Islands, Washington, *in* Howell, D.G., and McDougal, K.A., eds., Mesozoic Paleogeography of the Western United States: Pacific Coast Paleogeography Symposium 2: Pacific Section, Society of Economic Paleontologists and Mineralogists, p. 117–132.
White, C., Gehrels, G.E., Pecha, M., Giesler, D., Yokelson, I., McClelland, W.C., and Butler, R.F., 2016, U-Pb and Hf isotope analysis of detrital zircons from Paleozoic strata of the southern Alexander terrane (southeast Alaska): Lithosphere, v. 8, p. 83–96, https://doi.org/10.1130/L475.1.
Woodhead, J.D., and Hergt, J.M., 2005, A preliminary appraisal of seven natural zircon reference materials for in situ Hf isotope determination: Geostandards and Geoanalytical Research, v. 29, p. 183–195, https://doi.org/10.1111/j.1751-908X.2005.tb00891.x.
Wright, J.E., and Grove, M., 2009, Antler orogeny: Geological Society of America Abstracts with Programs, v. 41, no. 5, p. 12.
Wright, J.E., and Wyld, S.J., 2006, Gondwanan, Iapetan, Cordilleran interactions: A geodynamic model for the Paleozoic tectonic evolution of the North American Cordillera, *in* Haggart, J.W., et al., eds., Paleogeography of the North American Cordillera: Evidence For and Against Large-Scale Displacements: Geological Association of Canada Special Paper 46, p. 377–408.
Yokelson, I., Gehrels, G.E., Pecha, M., Giesler, D., White, C., and McClelland, W.C., 2015, U-Pb and Hf isotope analysis of detrital zircons from Mesozoic strata of the Gravina belt, southeast Alaska: Tectonics, v. 34, TC003955, https://doi.org/10.1002/2015TC003955.